PNAS
www.pnas.org

Supplementary Information for

Male mastodon landscape use changed with maturation (late Pleistocene, North America)

Joshua H. Miller[a,1*], Daniel C. Fisher[b,c,1*], Brooke E. Crowley[a,d], Ross Secord[e,f], Bledar A. Konomi[g]

Affiliations:

[a]Department of Geology, University of Cincinnati, Cincinnati, OH 45221, USA.

[b]Museum of Paleontology, University of Michigan, Ann Arbor, MI 48109, USA.

[c]Department of Earth and Environmental Sciences, University of Michigan, Ann Arbor, MI 48109, USA.

[d]Department of Anthropology, University of Cincinnati, Cincinnati, OH 45221, USA.

[e]Department of Earth and Atmospheric Sciences, University of Nebraska-Lincoln, Lincoln, NE 68588, USA.

[f]University of Nebraska State Museum, University of Nebraska-Lincoln, Lincoln, NE 68588, USA.

[g]Department of Mathematical Sciences, University of Cincinnati, Cincinnati, OH 45221, USA.

[1] J.H.M. and D.C.F. contributed equally to this work.

*Co-corresponding authors: Joshua H. Miller; Email: josh.miller@uc.edu

Daniel C. Fisher; Email: dcfisher@umich.edu

This PDF file includes:

Other supplementary information for this manuscript includes the following:

Datasets S1 to S2

1. Supplementary Materials and Methods

a. Overview of the Buesching mastodon

The mastodon analyzed here was discovered in 1998 during peat harvesting operations on property belonging to Buesching's Peat Moss and Mulch, Inc., Fort Wayne, Indiana. Initial stages of the excavation were overseen by Edward Smith, then on the faculty of Indiana University/Purdue at Fort Wayne (IPFW), with assistance from John Weddell and Sarah Surface. The specimen was borrowed for study at the University of Michigan and later returned to the Indiana State Museum (INSM), where it was donated and subsequently accessioned as INSM 71.3.261. 3D surface models of its skeleton (with replacements for missing bones) may be viewed on the University of Michigan Online Repository of Fossils website (http://umorf.ummp.lsa.umich.edu/wp/wp-content/3d/bonePicker.html?name=Buesching).

Widga and colleagues (1) reported an age of 11,450 ±110 radiocarbon years before present (^{14}C years BP) for this specimen (University of Arizona AMS Laboratory, AA100650). For this specimen, their table S4 lists the "Catalog #" as "INSM 98-L-SCA-E." In their reported catalogue designation, "98" (referring to the

year of discovery) was an informal identifier assigned by IPFW before the specimen was donated to INSM, and L-SCA-E was a label for fragment E of the left scapula of the Buesching mastodon, to which INSM assigned the number 71.3.261 (as noted above and in our main text). The date obtained by Widga and colleagues is consistent with, though slightly older than, a date that we obtained in 2004. The sample we dated was dense cortical bone from the medial surface of the specimen's right scapula. Our sample was trimmed to remove exposed bone that could have been subject to contamination during transport or handling and submitted to Beta Analytic, Inc. for AMS dating. Collagen was extracted and subjected to alkali pretreatment by Beta Analytic. Our reported conventional radiocarbon age (Beta-190885) was 11,280 ±70 ^{14}C years BP. Combining both dates (using the R_Combine function in OxCal 4.4 and IntCal20), the two dates establish a mean calibrated date of 13,220 cal BP (X^2 test: df = 1, T-statistic = 1.7), with a 95% probability distribution ranging from 13,316 to 13,111 cal BP. The preservation of the specimen is generally excellent, indicated by the previously reported carbon:nitrogen ratio (C:N = 3.3) (1). See Supplementary Discussion 2h for additional information on preservation and isotope biogenicity.

Studies of sexual dimorphism in mastodons (2–4) show that linear dimensions of skeletal elements of males exceed those of similar-age females, with differences often on the order of 20%. Based on measurements of the Buesching mastodon's tusks and long bones, and observations of epiphyseal fusion, it is recognized as an adult male (2–4). The development of, and wear on, its mandibular dentition places this individual in Laws' (5) Age Group XXI (http://umorf.ummp.lsa.umich.edu/wp/wp-content/3d/viewer.html?name=B_MAN_20), one relative-age category younger than the Hyde Park mastodon (3), to which we compare it below.

We focused most of our analysis on the right tusk of the Buesching mastodon, which is 290 cm long along its outer (convex) curve, with a maximum tusk circumference of 55 cm (Fig. S1; http://umorf.ummp.lsa.umich.edu/wp/wp-content/3d/viewer.html?name=B_R_T). The left tusk of this animal is shorter (265 cm long along its outer curve), due to tip breakage during the animal's life (presenting as a fracture scar abraded by use-wear; http://umorf.ummp.lsa.umich.edu/wp/wp-content/3d/viewer.html?name=B_L_T). Because tusks grow longer by adding material at their base (or proximal end), any material at the tip must have formed early in life. The loss of such material from the left tusk means that it lacks some of the record of early years that remains on the right tusk.

Most skeletal elements of this mastodon are in good condition, having been preserved in lacustrine sediments dominated by organic-rich marl and overlain by peat. However, a notable instance of damage is a circular puncture, 4-5 cm in diameter, located deep within the recess of the right temporal fossa, on the ventrolateral aspect of the cranium (near the jaw joint). The crisp margin of this puncture (illustrated previously (2; figure 4.2b)), with no evidence of either healing or subaerial weathering of the bone, offers strong evidence that the damage was perimortem (produced close to the time of death).

b. Tusk stabilization and preparation

Both tusks of the Buesching mastodon were recovered in situ, undisturbed by excavation activity related to peat harvesting. The tusks were both out of their alveoli (sockets) in the skull but located close to one another at the site and roughly parallel to one another, with tips pointing in the same direction. The left tusk was in one piece, except for delamination of some of its cementum (a relatively thin layer of mineralized tissue originally present on the outer surface). In life, cementum covers the dentin of the tusk, which is the main component of tusk mass. The left tusk was removed from the site and wrapped in a tarp for transport. The right tusk also had some cementum delamination and was already cracked, but not separated, along a compound fracture located just distal to the former gumline. While exposing this specimen, it became clear that it had almost separated into three pieces, two longer fragments, distal and proximal, and one smaller piece from the middle of the tusk. These pieces were removed separately and wrapped in polyethylene for physical protection and to prevent excessive loss of moisture during transit. Both tusks were brought to the University of Michigan, where they were cleaned in fresh water, stood on end to drain, covered by a polyethylene “tent”, and allowed to dry slowly.

Because the left tusk was most intact, we left it as unmodified as possible, continuing slow, closely monitored drying to minimize the chance of either mold development or fracturing (due to shrinkage of collagen in the dentin resulting from water loss). The right tusk was a better candidate for life history analysis because it was longer and retained a more complete record of the animal’s early years. Such analysis requires access to the tusk’s interior to sample all available years in convenient relative positions for serial sampling. In addition, having observed multiple tusks fracture on drying, we chose a protocol developed previously, using longitudinal cuts as both a means of sampling and a strategy for stress release, so that drying would be less likely to cause new fractures. After approximately two days of initial drying, the right tusk was longitudinally sectioned from tip to base, using a custom-modified, low-speed bandsaw with a half-inch-wide bimetal blade. This cut followed a path just lateral to the tusk axis. The cut began at the tusk tip and proceeded toward the break near the gumline. Approaching this position, the small fragment that belonged here was fitted onto the larger distal fragment, and the cut was extended. Passing through the second fragment, the third (proximal) fragment was fitted into place so the cut could continue. The first two fragments were then removed from the saw, and the cut was finished on the third fragment.

Following completion of the first cut, we repeated the process, making a second cut that was displaced medially from the first by 8-10 mm, to produce an axial slab that spanned the entire length of the tusk. This slab contained the tusk axis and dentin that had formed during most of this individual’s lifetime. Because the slab contained most of the moisture it had held at the time of discovery, and moisture content tends to promote visual discrimination of zones of dentin that differ in physical or compositional properties, it was relatively easy to trace zones of distinctive dentin properties across the freshly cut surfaces of the axial slab. The dominant pattern consisted of an imbricated sequence of V-shaped

domains, with the apex of each V pointing toward the tusk tip and the limbs of each V stretching toward the proximal end of the tusk. The regularity of this pattern was impressive, but equally so was the fact that these V-shaped domains paralleled the conical surface of the pulp cavity (Fig. S2c, d), where dentin apposition occurs. Each V-shaped domain presented a standard appearance – a light-dark couplet with a thicker layer of light-colored dentin toward the outside (obliquely facing the distal end of the tusk) and a thinner layer of dark-colored dentin toward the inside (obliquely facing the proximal end of the tusk). Since our earliest work on specimens like this, we have tested and corroborated the hypothesis that these repeating light-dark couplets represent years, and with additional studies targeting season of mineralization, we have argued that light-colored dentin represents spring through early winter, and dark-colored dentin represents late winter (6). Winter-spring boundaries typically present the most abrupt transitions in dentin properties (discussed further below), so we use them to demarcate years.

After the axial slab had been separated from the rest of the tusk, but while it was still wet, we marked and enumerated tusk years (from one winter-spring, W/S, boundary to the next) starting with the earliest-available year (near the tusk tip) and continuing all the way to the pulp cavity. We also added location reference marks every 10 cm from the tusk tip, measured along the ventral edge of the slab, which closely approximated the outside curve of the tusk. The axial slab was then wrapped loosely in polyethylene and monitored closely. Because it had a larger surface area to volume ratio than the remaining tusk "halves" (i.e., what remained after removal of the axial slab), it dried more quickly and with less fracturing. The medial and lateral "halves" of the right tusk, like the axial slab, were wrapped in polyethylene and monitored through slow drying, matching the approach used on the left tusk. As cracks on all of these larger specimens opened up, they were stabilized with epoxy pours. Larger cracks were sealed with epoxy putty, and the separate fragments of medial and lateral "halves" were assembled using epoxy.

When the axial slab was completely dry, it was embedded in epoxy and cut into segments for easier handling and storage. We started with a transverse cut that was 8 cm from the tusk tip and perpendicular to the tusk axis. Due to the geometry of tusk structure, such a cut could not be simultaneously perpendicular to all layers of dentin that it transected, but the transverse cut simplified access to both ventral and dorsal parts of the tusk growth record. This was important because the only remaining trace of the earliest year in the tusk (tusk year 1) was along the dorsal surface of the tusk tip (Fig. S1a); the ventral portion of the same annual increment had been stripped away by abrasion of the ventral surface of the tusk. For the same reason, dentin from tusk years 2 and 3 was only available from the portion of the axial slab dorsal to the tusk axis. For all other years, we focused on tusk layers located ventral to the tusk axis. This is because each year's accumulation of dentin tends to be thicker on the ventral side of the axis (due to the asymmetry of the curved stack of dentin cones and their V-shaped domains discussed above), increasing the structural and temporal resolution of the record in this location. Analysis of tusk growth within years is best done on

transverse thin sections (locations indicated by "TS" in Fig. S1c) that provide microscopic access to sub-annual dentin increments demarcated by second-order (fortnightly) features and third-order (daily) features (6–8), the analysis of which is summarized below.

To evaluate parts of the tusk proximal to the tip, the axial slab was cut into additional segments that were each about 20 cm long (e.g., from 8 cm to 25 cm behind the tip, from 25 cm to 45 cm behind the tip, and so on; Figs. S1c, d). These segments were separated from the rest of the axial slab by a pair of cuts on each end of the segment. The first cut extended from a selected point (e.g., 25 cm from the tip, measured along the ventral edge of the slab) and ran perpendicular to dentin layers, dorsally and proximally to the tusk axis. The second cut extended from the dorsal edge of the slab, again running perpendicular to dentin layers, until it met the first cut at their common termination along the axis (i.e., this cut had to be laid out from its endpoint, where the first cut met the tusk axis, to its point of initiation; the cut was then executed in the opposite direction). The two cuts that defined the proximal end of the segment extending from 25 cm from the tusk tip to 45 cm from the tusk tip were made in the same fashion, starting from a point on the ventral edge of the axial slab 45 cm from the tusk tip, running dorsally and proximally, perpendicular to dentin layers. The initiation point for the second cut was then chosen so that it could run perpendicular to dentin layers and terminate where the first cut in this pair met the tusk axis. This cutting plan continued proximally to the last such segment, from 185 cm to 202 cm behind the tip, which provided access to the distal portion of the pulp cavity. The exact apex of the pulp cavity was about 179 cm from the tip (measuring from a position projected to the ventral edge of the axial slab, Fig. S1c). From this position to the proximal margin, dorsal and ventral portions of the axial slab were separate moieties, one dorsal and the other ventral to the pulp cavity, each of which tapered gradually to the proximal end of the tusk, 290 cm from the tusk tip. Locations of thin sections and other samples are discussed below.

c. Serial sampling tusk dentin for isotopic analysis

Proboscidean tusk dentin forms throughout life by apposition along the surface of the conical pulp cavity (4, 8, 9). As this process progresses, the surface of the pulp cavity is displaced locally inward, toward the center of the pulp cavity, and proximally, toward the tusk base (4). The animal's life, and the tusk's growth history, is thus recorded in the sequence of layers that can be traced from near the tip of the tusk to its base (7).

Many studies based on serial sampling use samples from growth sequences that show no indication of timescale prior to analysis of sample compositions. However, approximate positions of year boundaries in mastodon tusk dentin are associated with visible cues (the light-dark couplets described above) that allow us to target specific portions of individual years or of the entire life history. The samples of dentin we used were obtained from two separate locations on the right tusk, each representing a different interval of time several years in length. These intervals were chosen because we expected them to offer

special insights into changes in mobility that might accompany significant junctures in this animal's life history.

Our ontogenetically earliest target interval was the adolescent period, which starts well after the completion of weaning (10). We mark adolescence as beginning just before the time when the young male left the matriarchal family unit and extending through several years until he had more or less adjusted to life on his own. In previous studies (2, 3), the year of separation (or "eviction") of young males from the matriarchal family unit has been associated with a distinctive pattern of annual variation in tusk growth seen only in males. Detailed analysis of this pattern requires microscopic assessment of dentinal lamination, but higher-level reconnaissance can be accomplished through measurements of annual increments of tusk length, or "Annual Extension Length" (AEL). Details of this measurement are presented below, but the general idea is that separation from the matriarchal unit is one of the most stressful times in the life of a young male. It comes immediately on the heels of some of the best years of his young life, when his access to food, water, and the protection of the family unit was a priority of his mother and aunts, one of which would likely have been the unit matriarch. This expectation clearly presumes that mastodons had a social structure like that seen in extant elephants (10), but this interpretation has already been proposed based on similarities in tusk dimorphism (4) and contrasting trackway associations (7). Years just prior to separation generally show successively higher values of AEL, and the year of separation generally shows a marked drop in AEL. The 2-3 years following separation typically show progressive recovery in AEL until the young male returns to his pre-separation growth trajectory. Based on values of AEL (Fig. S3, Dataset S1), we identified tusk year 9 as the probable year of separation. This year shows the greatest year-to-year drop in AEL prior to what is clearly the adult portion of life. The age of the Buesching mastodon during the formation of this part of the tusk (estimated as 12 years old; see Supplementary Discussion 2b-d) is also consistent with ages-of-separation reported for other male mastodons (Fig. S3, boxplot). Focusing on year-to-year differences in tusk AEL raises the question of what to make of the somewhat low values for this variable in tusk years 6 and 7? To understand these, we first turn to the raw data in Dataset S1. Raw values for AEL in these years are in fact not small (14 cm and 11 cm) for this tusk, though they are markedly less than the AEL value of 17.5 cm for tusk year 5, a value that is the largest in the entire tusk. What makes AEL for year 5 so high?

The pattern of variation in AEL is controlled both by variation in the rate of tusk growth during the years in which particular annual layers formed and by variation in the intensity of abrasion acting to remove portions of the tusk surface, later in the animal's life. In short, abrasion that removes part of the tusk surface can change the outcrop pattern of boundaries between tusk years, shifting the landmarks used to measure AEL. Examining this process more closely, at any given point along the tusk surface, abrasion first affects cementum and then, if cementum is removed, it attacks underlying dentin. Abrasion also tends to be most intense near the tip of the tusk and diminishes in intensity away from the tip, because in normal use, most of the tusk's contacts with abrasive substrates are

initiated at or near its tip. In addition, for a given distance from the tip, such contacts typically involve greater impact and frictional forces along the ventral, outer curve of the tusk than along the dorsal surface. These generalizations are supported by the pattern of dentin exposure illustrated in Fig. S1a, where all cementum has been removed dorsally, near the tip, and ventrally, from the tip all the way back to the exposure of tusk year 16. The bounding surfaces that represent the beginning and end of any given year within dentin structure have proximal-most positions that are initially located just inside the cementum-dentin junction (CDJ), but from there, they extend distally, and progressively deeper into the tusk, following the slope of a former surface of the pulp cavity, all the way to the tusk axis. If cementum just outside one of these year boundaries is abraded away, exposing some of the outermost dentin, continued abrasion removes that outermost dentin, shifting the outcrop of that year boundary distally on the abraded surface of the tusk. A consequence of this abrasion is that surface traces of year boundaries are systematically shifted distally, especially along the outside curve of the tusk, where abrasion tends to have been most pronounced.

Returning to Fig. S1a, measurements of AEL quantify the distance between the beginning and end of a given year, exposed along the tusk surface. We generally make tusk length measurements along the outside curve of the tusk because fitting a flexible (fiberglass, non-extensible) tape to this convex curve maximizes repeatability. However, all year boundaries exposed along the highly abraded outer curve of the tusk have been displaced distally (by that abrasion) and thus misrepresent the original positions of those boundaries. We therefore trace boundaries from severely displaced positions on the outer curve, to locations where they are less severely displaced, on the medial or lateral flank of the tusk. This attempt to measure boundary positions where they are least displaced may even continue to the dorsal aspect of the tusk. No matter where year boundary positions are located, it is critical to express their locations using a single, stable reference system, for which we use the outer curve of the tusk. Abraded or not, this is the easiest place to make repeatable measurements of distance from the tusk tip. We quantify annual boundary positions by first finding their most proximal locations on the tusk. From those points, we project (along lines perpendicular to the tusk axis) across the tusk to the outer curve, and then measure distances from the tusk tip along that curve.

Examining the surface traces of year boundaries in Fig. S1a, those separating tusk years 1-3, with their positions shifted distally by extensive abrasion of the ventral aspect of the tusk tip, show up as sweeping arcs that do not even extend to the outer curve of the tusk profile. However, this is immaterial for AEL, for which we (a) marked the proximal end of each trace where it crossed the dorsal profile, (b) projected this position to the ventral profile, and (c) measured its distance from the tusk tip along the ventral curve. The proximal boundary of tusk year 4 is the first to extend to the outer curve, leaving this year (as a whole) with a ventral exposure that extends all the way to the tip and a dorsal exposure that is narrower (with the dorsal exposure of both its boundaries shifted distally by abrasion). The proximal boundary of tusk year 4 is also the distal boundary of tusk year 5, and as noted above, it has been shifted distally,

but the proximal boundary of tusk year 5, traced dorsally, finally disappears under the distal-most remnant of cementum on the tusk. This is the first year boundary that clearly has an unabraded portion (under cementum) that has not been displaced by abrasion. With its posterior boundary “pinned” in this way, and its anterior boundary shifted distally, AEL for tusk year 5 exaggerates its rate of growth. As for the following two years, tusk year 6 is the first year in the tusk to have both the boundary marking its beginning and the boundary marking its end terminate under cementum, giving us a value for AEL that is not affected by abrasion. Likewise, all subsequent tusk years share this property. As noted above, neither tusk year 6 nor 7, viewed from the perspective of raw AEL values, represent times of notably reduced growth, and tusk year 8, rebounding to an AEL of 13.5 cm, is precisely what we normally see just before the year when a male calf departs from the matriarchal unit. By comparison, tusk year 9’s AEL value of 8.5 cm, especially given that both years 10 and 11 follow with higher AEL values of 9.5 cm, draws attention to tusk year 9 (when the mastodon was 12 years old; Supplementary Discussion 2b-d, where we argue that for this individual, age = tusk years + 3) as the best candidate for the year of incipient independence from the matriarchal unit.

Despite this judgment, we feel obliged to discuss the reduction in extension rate in tusk years 12 and 13, if only because most male tusks have only a single pronounced drop in growth rate in the part of the tusk associated with adolescence. Is there any chance that this later interval represents the time of separation from the matriarchal unit? We suspect not. In addition to being less dramatic than the drop in tusk year 9, the sequence of AEL values in tusk years 11-14 shows a less typical trajectory than we see in tusk years 8-11. Moreover, only the drop in tusk year 9 matches the general timing of independence identified in other specimens of male mastodons (2, 9). Admittedly, making this judgment requires assessing how tusk years translate to actual ages (discussed below), but this exemplifies the holistic approach to reading life history that we consider essential. For this tusk to be consistent with an age of maturation as late as 15 (12 + 3; maturation at this late an age might indeed be expected under conditions of environmental stress), we would have expected a lower overall growth rate (2).

Our interest in the time of separation from the matriarchal family unit and its aftermath led us to prioritize tusk years 9-13 for serial sampling. Ideally, we would have included at least one year on each end of this sequence (i.e., tusk years 8-14), but because tusk years 12 and 13 were at least somewhat unusual (Fig. S3, Dataset S1), showing tusk extension rates lower than normal for this time of life (3, 9), we felt compelled to include them and part of the following year in our sample. We thus decided that sampling at least some of year 14 was more important than sampling tusk year 8. Our target interval for sampling adolescence thus became tusk years 9-14.

Since each year in a tusk is exposed on the axial slab in a wide range of positions, from the axis to the cementum-dentin junction, it might at first seem that our choices for where to sample a given year are relatively unconstrained. However, for sampling a series of years, milling a continuous sequence of

samples, each with structural control (i.e., following dentinal lamination) is the only way to conduct our analyses and still avoid time gaps and minimize time-averaging between consecutive samples. On the other hand, a seven-year sequence (years 8-14 inclusive, our ideal target as described above) is almost more than can be obtained at one position along the tusk. This is especially true given that years are not constant in their thickness along their entire extent from axis to cementum-dentin junction (CDJ). Instead, they taper markedly on approaching the CDJ and somewhat, if less conspicuously, in proximity to the axis (11). To avoid sampling a year where it was thinner than it was elsewhere on the tusk, we tried to be sure that (a) the ontogenetically youngest year in the sequence was at least two years away from (inside of) the original CDJ (the location of which had to be estimated where abrasion of the tusk during life had removed cementum), and (b) the oldest year was at least two years from the tusk axis. It was also critical to choose a region where the dentin was not greatly interrupted by desiccation fractures. To conduct isotopic sampling of tusk years 9-14 under the constraints discussed above, we selected the segment of the axial slab that extended from about 45 to 64 cm from the tusk tip. From this segment, we cut a sample block (SB-A in Fig. S1c) that was about 8 cm long (parallel to the tusk axis), from 56 cm to 64 cm from the tusk tip.

We prepared the sample block containing our targeted sequence of years by completely sanding the epoxy off one surface (the medial face of the axial slab), using a graded series of dry, abrasive papers (100, 320, and 600 grit). This left a smooth, solid surface on which second-order (fortnightly) incremental features could be viewed under a stereoscopic microscope and used as reference lines to guide acquisition of serial samples. The longitudinal saw cuts that produced the axial slab were almost exactly perpendicular to layering in the dentin (meaning that dentin layers extended into this block at 90° to the polished surface, not at some other angle). We therefore kept the polished surface of the sample block horizontal, drilling into it with a vertically mounted, stationary, high-speed dental drill. To accomplish this, we mounted the sample block on a rigid sheet of acrylic, which could be slid easily on a horizontal, vertically adjustable stage positioned under the drill. To avoid interference between the drill and the associated stereomicroscope, the optic axis of the microscope was inclined. Sampling began by raising the stage until the spinning bit engaged the polished surface of the block. The stage was then locked at this level, and the acrylic sheet carrying the sample block was slid horizontally, “driving” the spinning bit along a single set of incremental features visible on the polished tusk surface. In terms typical for a manufacturing setting, this process would be described as “milling” rather than “drilling.” Coming to the end of a mill path, the stage was lowered and sample powder was transferred to clean, labelled vials using nitrogen-free weighing-paper and a fine brush. Several passes along a single mill path were generally needed to collect our required 60-90 mg of dentin. After collection, powder from a single serial sample (i.e., a single mill path) was homogenized and then dispensed as two aliquots, the first for $\delta^{18}O$ analysis and the second for $^{87}Sr/^{86}Sr$ analysis. The results of these two analyses constituted a linked pair of paleoecological proxies (reflecting season of mineralization and

place of mineralization, respectively), united by their derivation from a single mill path, harvesting dentin powder that had mineralized during a single interval of time, during which the animal occupied some likely-complex and yet-to-be-determined portion of the landscape. Between consecutive serial samples, the entire sampling area and brush were blown free of powder using carbon dioxide at 30 lbs. pressure.

By orienting the bit to penetrate the tusk within the plane of dentin increments, time-averaging was minimized in the depth direction (i.e., depth of plunge of the bit), but some time-averaging in the direction of the width of the mill path (i.e., the direction of dentin apposition) was unavoidable, given our targeted sample mass. We milled samples using a 1-mm-diameter diamond burr, so if the first sample collected for a given series was located in the middle of a sample block, it had to be acquired by plunging the bit into the unblemished sample slab. Such a sample was necessarily 1 mm wide. In fact, because of modest eccentricity in bit rotation, and because we had to travel this path several times at successively deeper levels to collect the required sample mass, the final width of such a path would be somewhat greater.

Before starting the milling process, it was hard to know what sample spacing would be practical and therefore what time interval would be covered by the 36 samples that are usually our limit for one batch of samples, under normal pretreatment procedures. For the adolescent dataset, our trade-off between temporal resolution and temporal coverage meant that milling extended mostly (but not entirely) through the ninth year. Although we had originally hoped to include tusk year 8, extending the sequence that far back in time would have brought us too close to the estimated position of the CDJ (i.e., where it was located, before abrasion of cementum from this part of the tusk) and would have yielded a suite of samples too large to have been processed in one sample set, under optimally standardized conditions. Our sequence covering the adolescent years thus consists of 36 serial samples covering about 5.5 years (tusk years 9-14) at an average temporal resolution of about 6.5 samples per year (Dataset S2).

Sampling the Buesching mastodon's adult years near the end of his life would have been possible anywhere along the surface of the pulp cavity at the time of death. However, applying criteria discussed above for prioritizing locations where target years are thickest, we chose a section removed from both the tusk axis and the CDJ. Working near the proximal end of the tusk, this translates into avoiding locations that are either near the apex of the pulp cavity or near the proximal margin of the tusk (3). This sampling strategy can also be described from a more developmental perspective. It directs us to avoid dentin formed by newly differentiated odontoblasts and dentin formed by odontoblasts nearing the end of their effective lifespan (3). We selected a region on the ventral portion of the axial slab (outer curve of the tusk), cutting a sample block (SB-B in Fig. S1d) that extended from 233 cm to 239 cm from the tusk tip. Again, we polished the medial face of the axial slab to remove epoxy from its surface and prepare it for serial sampling. However, in this tusk region, there were two geometric challenges. The first was that the cross-sectional shape of the pulp

cavity here was elliptical (in contrast to the more circular cross section displayed by dentin layers in the distal part of the tusk; this difference is normal), with a major axis inclined relative to the plane of the major curve of the tusk. Because of this, the pulp cavity surface was oriented locally at about 70º (in a dorsolateral direction) to the plane of the axial slab, rather than 90º. This meant that dentin layers extending into the thickness of the sample block would be similarly oriented. To address this, the sample block for the adult years at the end of life was mounted on *two* acrylic sheets, with the upper one hinged (near the pulp margin) to allow it to rotate relative to the lower one. We then secured the upper sheet 20º above the lower sheet, so that dentin increments were oriented vertically, minimizing time averaging in the direction in which the sampling bit plunged into the sample block.

An additional challenge to sampling the final adult years is that appositional thickness is lower (i.e., years are thinner) than earlier in the animal's life, even if they are sampled in an optimal position relative to the apex of the pulp cavity and the proximal margin of the tusk. To retain as much temporal resolution as possible, we adjusted our procedure to sample on a tighter spatial scale. As we had done for the adolescent years, we conducted our sampling in reverse temporal order, but in this case, our rationale was different. Starting from the surface of the pulp cavity, which assayed the end of life, permitted us to make use of the open pulp cavity, in which the bit could spin freely. This allowed the first sample we acquired to be collected using less than a full bit width. Continuing in this fashion, we milled 30 samples, with an average mill path width of about 0.5 mm (Fig. S2b). In this way, we sampled from what would have been early in year 32 in the tusk, backward in time through most of year 29. This covered a span of about 3.5 years, sampled at a resolution of about 9 samples per year (Dataset S2).

To estimate the time (months of growth) represented by each serial sample, we divided their mill path widths by the fraction of tusk year sampled. Most tusk years were completely sampled; thus, this calculation was simply serial sample width divided by the pooled widths for that year. For incompletely sampled tusk years (9, 14, 29, and 32), serial sample widths were standardized to the fraction of year sampled before dividing by the pooled widths. We estimate that we sampled three-quarters of tusk year 9, half of tusk year 14, and half of tusk year 32 (Fig. 1). For the purposes of these calculations, we estimate that approximately the entire year of tusk year 29 was sampled. Our calculations assume growth rate is constant throughout the year. While this assumption is somewhat crude (dentin apposition rates during summer months are higher than during winter months (8, 9, 12), it is a useful and simplifying approximation for our purposes. Further, because our current calculations may overestimate the duration of growth represented by warm-season serial samples (i.e., inflating the denominator), we are ultimately erring in the direction of more conservative estimates of Buesching mastodon movement rates (km moved per month) during periods of maximum potential activity.

It would, of course, have been possible to add sample series between the blocks of tusk and time that we used to assay adolescence and the terminal

portion of adulthood. However, to match our criteria for temporal precision and to ensure a continuous record, we would have had to devote yet more samples to ensure adequate overlap between sequences derived from different portions of the tusk. We have addressed such issues in prior studies of complete tusks (e.g., both male (3) and female (11)), but we considered the objectives of the current study to be best satisfied by our more targeted approach.

d. Isoscape for referencing serially grown tissues

The error of the $^{87}Sr/^{86}Sr$ isoscape in estimating the locations of formation of serially formed, mineralized tissues of mastodons and other megafauna is unknown. However, previous work has indicated that modeled values of $^{87}Sr/^{86}Sr$ for specimen collection sites can be good predictors of measured $^{87}Sr/^{86}Sr$ of time-averaged tissues (e.g., bones and bulk samples of teeth), particularly for mammals over 100 kg (13). To date, there has not been a study evaluating the efficacy of the isoscape for reconstructing the provenance of skeletal features with higher temporal resolution (*e.g.*, tusks, antlers). An important additional control on inaccuracies in modeled $^{87}Sr/^{86}Sr$ isoscapes is the geologic complexity of the terrain (13–15). Indiana and surrounding states generally have low geologic complexity, providing a relatively simple landscape across which to evaluate biologically available $^{87}Sr/^{86}Sr$. While isoscape error for estimating location of tusk-recorded mastodon resource consumption remains unknown, the low geologic complexity of our target regions and large body size of mastodons appears to be a best-use scenario for applying this isoscape. Further, given our sampling and analytical strategies, observed differences between adolescence and adulthood should be informative of changes in patterns of landscape use associated with this phase of ontogeny.

2. Supplementary Discussion

a. Tusk structure as a record of life history

The right tusk provides the most complete record of life history events for the Buesching mastodon. At their earliest stage of formation, proboscidean tusks (which are incisor homologs) consist of a diminutive crown, but this transitions into an ever-growing root that comes to dominate the tooth as a whole. Both crown and root are mainly formed of dentin, although the crown is covered by a layer of enamel, and the root is covered by a layer of cementum. Each of these types of mineralized tissue has a fundamentally laminar structure, but the organization and rhythmic character of dentinal layers have received most study (7). Dentinal lamination is hierarchical, with first-order (annual) layers being the largest-scale increments, and second-order (fortnightly) and third-order (daily) layers successively nested within years (8). In an adult tusk, the distal extremity has typically been lost by breakage or abrasion, usually operating as a succession of events of varying scale and continuity. Abrasion tends to be concentrated on the flanks of the tip and along the outer curve of the tusk, where there is frequent contact with the ground surface, vegetation, and other abrasive substrates in the environment. Fractures occur most frequently near the tusk tip,

during activities such as digging for water, breaking branches to acquire twigs and leaves, stripping bark from trees, and defensive or offensive encounters. As a result, the tusk of an adult typically has a blunt, polished tip and outer curve, from which cementum and some dentin have been abraded (9). On close inspection, this smooth dentin surface displays an oblique cross section through first-order (annual) increments. Each annual increment includes a lighter zone (representing warm-season growth) and a dark-colored zone that forms near the end of winter or early spring (12). These dark zones, and associated structural and compositional features, are the most easily recognized temporal cues within the dentin sequence, and we therefore track time within ontogeny by marking years from one winter-spring (W/S) boundary to the next. Years recognized in this way are diagrammed in Fig. S1a and b.

b. Inventory of tusk years

The first step in reconstructing life history is to enumerate years preserved in the tusk (i.e., “tusk years”). We have already noted that this can be done by tracing and counting years along the freshly cut surfaces of the axial slab, but we have also conducted an independent count by focusing on external features. The tusk of an adult invariably begins with an incomplete year that is terminated by a W/S boundary but begins, judging from its thickness, less than a year earlier; this is the first tusk year (we deal below with the question of how old the animal was during apposition of this increment). In the right tusk of the Buesching mastodon, this first tusk year is represented only by a thin “saddle” of dentin on the dorsal aspect of the tusk near its tip (Fig. S1a). All subsequently-formed years are located adaxially and proximally relative to this year. The second and third tusk years are distinguished by similar outcrop patterns on the tusk surface, because like the first year, the distal and ventral portions of their original conical configuration have been removed by abrasion. In contrast, year 4 may be traced all around the tusk because at least some portion of each radial sector of its original cone remains. Tusk years 4-15 show distinctively sinuous W/S boundaries that reflect mainly distal displacement of the positions of these boundaries by removal of portions of the conical increments attributed to each year, modulated on a smaller scale by irregularities of the original surface of apposition. Counting tusk years through this zone of extensive abrasion is relatively straightforward.

Although features visible on the polished dentin surface suffice to distinguish annual dentin increments for tusk years 1-15, cementum abrasion has not been as extreme in more proximal locations on the tusk. Tusk year 16 only has a small area of dentin exposure on the ventrolateral aspect of the tusk (Fig. S1a), and years located still more proximally have no dentin exposure. Fortunately, we do not require dentin exposure to continue this externally-based count of tusk years. Another category of features that is often visible on the external surface of tusks is annual (or first-order) periradicular features. These are closely associated with W/S boundaries and are formed as deflections of the topography of the cementum-dentin junction (CDJ) that arise through retardation of the rate of dentin extension relative to the rate of dentin apposition during the

late winter, followed by an acceleration of extension again (relative to apposition) after the onset of spring (16). This syncopation of growth rate fluctuations generates a topographic irregularity that may be expressed either as a “shoulder” (resembling a geological monocline of the CDJ) or a “ridge” (resembling a geological anticline of the CDJ) that encircles the tusk. Although this topography reflects processes within the dentin, the relief that results is most pronounced at the level of the CDJ. To show this directly, Fig. S2c displays three first-order periradicular features (marked by arrows) on the polished, dorsal moiety of the proximal portion of the axial slab. For this image, we chose the lateral surface of the axial slab, because this is where periradicular features were most clearly exposed. In this image, cementum seen in longitudinal cross section is reddish brown, the CDJ is a dark line, and dentin in longitudinal cross section shows up as various shades of beige. When only a thin layer of cementum is present on the CDJ, as with the periradicular feature marking the beginning of tusk year 31, the expression of the feature at the outer surface of the cementum is pronounced. This periradicular feature is only about 10 cm from the proximal margin of the tusk (i.e., about 280 cm from the tusk tip, although this is a projection from the outer curve of the tusk). However, as we move to more distal locations on the tusk (compare the periradicular features at about 273 and 267 cm from the tip, near the beginnings of tusk years 30 and 29, respectively), we are dealing with surfaces that have existed for longer, and have had more time to accumulate cementum, which eventually covers and subdues the external expression of periradicular features. Following the process of cementum accumulation backward in time, to parts of the tusk that formed even earlier in this animal’s life, periradicular features still exist, but they become harder to recognize from the tusk exterior. By understanding and anticipating this gradient, we were able to continue counting years back to the beginning of year 23 (Fig. S1b). Several of these earlier years were bounded by only subtle periradicular features, as seen from the outer surface, and beyond this, near the alveolar margin, cementum reaches its maximum thickness (ca. 8 mm) anywhere on the tusk, leading to the greatest likelihood that periradicular features will be obscured beneath its thick mantle.

The upper limit on cementum thickness exists because tusk cementum forms only within the tusk alveolus. Once a given region of tusk surface erupts beyond the alveolar margin (or in soft tissue terms, beyond the gingival margin or gumline), cementum deposition ceases (at that locus), and the existing cementum surface is instead subjected to abrasion resulting from contact with the animal’s own food, the skin of his trunk (which may often be covered with fine-grain sediment), or bark and tree branches during foraging activities. Abrasion is even more effective at obscuring periradicular features than is progressive accumulation of cementum because abrasive processes are typically mediated by surfaces coming into contact with one another. Areas of positive topography (i.e., that protrude beyond surrounding regions) engage opposing surfaces before surrounding areas of lower relief and maintain contact longer. For this reason, from year 23 to year 14, we were not able to trace periradicular features across the abraded surface of cementum, but we were able to recognize

them in longitudinal section along the dorsal margins of the sawn tusk "halves". Moving even more distally than this, the remaining cementum on the dorsal surface of the tusk (gray region in Fig. S1a) was abraded enough that a new phenomenon emerged. In places where the laminar cementum draped over periradicular ridges, but had then been truncated to within millimeters of the sharply inflected CDJ, subtle color and texture lineation (exposed laminae) betrayed the presence of the periradicular feature below. This is the basis for tracing winter-spring boundaries as dashed lines from years 13 to 8, as if seeing through their dorsal cover of cementum (Fig S1a).

To conclude discussion of the number of years in the Buesching mastodon's right tusk, there is one important inconsistency to resolve. It appears in Fig. S2d that the last year of life was year 31, and it also appears, looking from the outside of the tusk, that the last part of this year was near the W/S boundary. However, examining this margin carefully, we found that dentin and even traces of cementum are broken off all the way around the specimen. We therefore made and studied a transverse thin section of dentin adjacent to the pulp cavity (from near the location of sample block SB-B). In this, we verified that dentin apposition continued past the W/S boundary at the close of year 31, and into the following spring or early summer – i.e., into the early portion of what would have been tusk year 32. In terms of tusk extension, this would have brought the proximal margin to a position suggested by the finely dashed line at the far right of Fig. S1b. The $\delta^{18}O_p$ profile discussed in our main text is consistent with this reconstruction, confirming that the entire tusk margin was broken away. This last bit of the tusk was not recovered at the site, but since this tusk (like its mate) was removed from its alveolus prior to deposition, the separation of this fragment from the rest of the tusk could have occurred before deposition of the tusk at the site where it was recovered.

In summary, the record of life contained in the Buesching mastodon's right tusk includes 30 complete years, tusk years 2-31, and two incomplete years, tusk years 1 and 32. The pattern of abrasion at the tip of the tusk suggests that tusk year 1 is simply the remnant of what was a complete year, the early portions of which were removed by abrasion, probably along with other years at the beginning of life. In contrast, tusk year 32 is only the beginning of a year that was interrupted by events associated with this animal's death. A minimal estimate of this animal's age at death is thus 31.

c. Years lost from the tusk tip (estimated age at death)

To estimate age at death, we need to compare this tusk with one that appears to retain a more complete record of its early years of life. The best comparative case would involve an individual that died at a younger age, before experiencing the vicissitudes associated with maturation, the cumulative effects of use of the tusk in foraging, and even more vigorous use of the tusk in intraspecific interactions associated with maintenance of position within a local dominance hierarchy and with contests over access to potential mates. A detailed analysis matching this design compared tusk structure of the Hyde Park mastodon, an adult male with 33 complete years in the longer of its two tusks

and a molar dentition indicative of Laws' relative Age Group XXII (the Buesching mastodon is just one Laws' Age Group younger) and the Heisler mastodon, a young-adult male with 16 complete years in the longer of its two tusks and a molar dentition indicative of Laws' relative Age Group XII (3). Assuming the Hyde Park and Heisler mastodons had tusks of similar morphology and growth trajectory, which seems reasonable for conspecifics of the same sex, we can estimate the amount of tusk missing from the Hyde Park mastodon by comparing tusk geometries and growth patterns. Through such comparisons, we find that the Hyde Park mastodon has lost at least 3 years and 33 cm of tusk length; that is, this many years and centimeters of length are present on the Heisler tusk distal to the position where its tusk radii and positions of W/S boundaries match those observed on the Hyde Park tusk. This conclusion came about in two steps, illustrated in Fig. S4:

1) The most distal exposure of a W/S boundary on the dorsal surface of the Hyde Park tusk is the boundary separating tusk years 1 and 2 (i.e., the 1-2 boundary). The dorsal surface at this point is abraded, but less so than this tusk's ventral surface, and the boundary is exposed at a dorsal tusk radius (i.e., distance from the axis) of 33 mm. An identical tusk radius characterizes the 3-4 boundary on the dorsal portion of the Heisler tusk, but this boundary position is overlain by intact cementum, so we know that it cannot have been displaced distally. If these two positions match, there must be a difference of at least 2 years and 22 cm of tip length between the Hyde Park and Heisler tusks. However, we cannot yet claim much confidence that these two positions really do match.

2) Looking more proximally on each tusk, the 5-6 boundary on Hyde Park (4 years proximal to the 1-2 boundary discussed in 1) occurs, just barely, under intact cementum at a dorsal radius of 52 mm. Again, an identical tusk radius, here securely under intact cementum, characterizes a boundary in the Heisler tusk, but in this case it is the 8-9 boundary, 5 years proximal to the 3-4 boundary discussed in 1). Because we know that neither boundary position has been displaced by abrasion in this case, identical dorsal radii suggest that they represent the same year in a morphologically conserved program of tusk growth. Thus, we have greater confidence in using this assessment of age adjustment, rather than argument 1), above, and estimate a difference of 3 years and 33 cm of tip length between the Hyde Park and Heisler tusks. The difference between the 4-yr and the 5-yr offset between successive measurement positions on these two tusks probably arose through unequal tip abrasion, but shows in any case that these correlations cannot both be valid.

The dimensions and configurations of annual increments in the Buesching mastodon's right tusk are remarkably close to those of the left tusk of the Hyde Park mastodon (3). Thus, a comparable estimate of time and tusk length lost

from the tip would apply to our current study. This means that tusk year 1 of the Buesching mastodon is likely at least the fourth year of life.

Adding 3 years to the 31 years already enumerated in the Buesching (right) tusk implies a minimum age of 34 years at death, or 2 years younger than the estimated age of the Hyde Park mastodon (3). This is, moreover, consistent with the difference in development of the cheek dentition between these two individuals, with Buesching (at Law's Age Group XXI) younger than Hyde Park by one relative age category. Although the absolute difference in years between successive Laws' Age Groups is not constant throughout the lifespan, a difference of 2 years between successive Age Groups is normal for adults (17).

d. Year of separation from matriarchal unit

Sexual maturation of male proboscideans is a two-phase process that has been observed directly in extant elephants (10, 18) and reconstructed using fossil evidence derived from extinct mammoths and mastodons (3, 7, 9). The first phase begins when a young male becomes physiologically sexually mature and begins to engage in styles of interaction with younger juveniles that are not tolerated by his mother or aunts. This leads his mother to intervene to disrupt this behavior and subsequently to evict the young bull, forcing him from the family unit. He may resist, following the matriarchal unit at a distance, too distressed to feed or drink normally and too inexperienced to locate resources on his own that are comparable to those he has enjoyed thus far in the protected environment of his family group. In this manner, the condition of the young male deteriorates until he gives up and strikes out on his own. Even so, recovery to the point of resuming his former growth trajectory is a process that can require two to three years, if not more.

As discussed above, one of the best external indicators of the condition of a proboscidean at various stages of its life is the magnitude of annual increases in tusk length. This level of detail is not always evident, but for Pleistocene specimens, close inspection is often rewarded. The key challenge in assembling records like this from various places on a tusk is to use a measurement system based on a common frame of reference. To measure "Annual Extension Length" (AEL), we need access to first-order (annual) incremental features that mark the beginning and end of each year, for which we use winter-spring boundaries. As discussed above (Supplementary Methods 1c), incremental features in dentin are conical in geometry, and if exposed on a surface and abraded, their outcrop locations shift distally. Well-controlled measurement of annual rates of tusk extension are only possible where W/S boundaries at both the beginning and end of a year can be traced to a point where they are covered by cementum.

Another complication in measuring AEL that was not discussed above is that the proximal margin of a tusk, and likewise the maximum proximal extent of any undamaged incremental feature, is often a sinuous curve that resembles the undulatory contour of the bony terminus of the alveolar socket where the growing end of the tusk resides during the life of the animal. Ideally, all critical incremental features would extend to the outside curve of the tusk, where their positions could be measured directly. However, some features of interest only retain

unaltered positions dorsally. In cases where a feature of interest is near the proximal margin of the tusk, we can sometimes use the sinuous margin itself, or nearby periradicular features, as a template for projecting a feature's location to the outer curve of the tusk. However, for features in the distal half of the tusk, where periradicular features rarely remain nearby as guides, we followed the projection protocol described above (along a perpendicular to the tusk axis), to measure distances of features from the tusk tip (Dataset S1). As indicated there, we interpret tusk year 9 (mastodon age 12) as the year of eviction (2, 3).

e. Age of onset of musth

The second major milestone in male maturation in elephantid proboscideans (following eviction from the family unit) is "musth", a hormonally regulated period of fasting, heightened aggression (18), and elevated mobility and probability of successful mating (19) that occurs in mature males on roughly annual intervals. We do not simply take it for granted that mammutid males displayed all the elements of musth typical of elephantids. Indeed, no mammutid fossils preserve soft tissue that would allow us to confirm (or rule out) presence of musth (temporal) glands. Nonetheless, microscopic analyses of sub-annual dentin increments in mammutids show that mature males, starting sometime in their early- to mid-20s, show a pronounced drop in rate of dentin apposition during spring and early summer that we interpret as a fasting period like that known for elephantid musth. Associated with this reduction in rate of dentin apposition is also evidence of tusk damage suggestive of male-male aggression such as that shown by elephantid males during conflicts over access to potential mates (2, 3). Younger males and females of all ages generally show increased rates of apposition at this season, consistent with access to forage of greater nutritive value than was typically available during winter. Whether the musth-like features of mammutid males are homologous to those of elephantids may still seem like an open question, but on examining traits of both groups, we are impressed by their profound similarity.

If we were intent on determining exactly when the Buesching mastodon exhibited onset of musth (or at least the musth-like patterns we have documented in other mammutids (3)), we would not have limited our sampling to adolescence and adult years near the end of life. However, onset of musth is, by its nature, a gradational process, and this would have committed us to a larger study than we felt was warranted at this early stage in our exploration of mobility. What we undertake in the paragraphs below is instead a high-level reconnaissance to address whether the pattern of tusk growth between adolescence and the final years of life resembles cases in which we have previously documented onset of musth. The observational basis for this discussion is patterns of variation in rate of tusk extension and other features that can be observed from the tusk exterior.

In prior sections, we discussed briefly the history of changes in AEL post-eviction. The recovery of tusk growth rate seen in tusk years 10 and 11 is entirely normal. The subsequent decline in growth rate in tusk years 12 and 13 is not normal, but it could relate to an injury that the young, but almost-adult male

sustained in the course of beginning to establish himself within a local dominance hierarchy, or to any number of other, unspecified, health or environmental challenges. There is no need to distinguish between these interpretations at present. In any case, tusk year 14 represents a turn for the better, and tusk years 15 through 22 represent solid investments in tusk growth that would be expected of a male approaching the onset of musth (18). The first hint of a change that might represent the onset of musth is the decline in AEL seen in tusk year 23. This could have been caused by the fasting associated with musth, or it could be a consequence of injuries sustained during battles fought during a novice male's first significant musth encounters. It is also possible that this change reflects a short-term deterioration of this animal's environment, but a similar decline (though slightly earlier in life) was observed in the Hyde Park mastodon (3) and was interpreted as the onset of musth. A comparable interpretation seems reasonable here, though further analysis would require microscopic evaluation of patterns of dentin apposition during this part of the tusk record.

We have described above how accumulation of cementum on the outside of the proximal portion of a tusk, still within its alveolus, progressively masks the topography of first-order periradicular features. In light of this, it might seem that any topographic feature on the exterior of the alveolar portion of a tusk might be similarly masked. However, one type of feature that is curiously not masked, even by advanced cementum deposition, is the pattern of arcuate arrays of pits just proximal to W/S boundaries (i.e., offset in the direction of dentin extension) during adult years in male mastodon tusks. Translating position of occurrence into season of development, the locations of these pits indicate development during spring. These features have been described as "cementum defects" on the Hyde Park mastodon (3). They were interpreted as reflecting damage to recently differentiated cementoblasts, when the ventral portion of the growing margin of the tusk was impacted into the bone surface at the back of the tusk alveolus, driven by a downwardly directed reaction force acting at the tusk tip. This localized impingement compromised the ability of this cohort of cementoblasts to deposit well-organized laminar cementum, permitting defects to propagate outward, even as cementum accumulated over periradicular topography. The downwardly directed reaction forces acting at the tusk tip were interpreted as associated with use of the tusk as an upwardly oriented thrusting weapon during battles between rival males for access to mates. In extant elephants, these types of battles occur only during episodes of musth. Musth occurrence in extant elephants is only moderately seasonal. However, there is evidence for greater musth seasonality near the end of the Pleistocene, which may have been a response to increases in selection forces favoring spring calving (2, 7). Given that proboscidean gestation periods approach two years in duration, spring calving would be consistent with musth, and hence conception, occurring predominantly in late spring to early summer (7).

As illustrated in Figs. S1b and S2d, the right tusk of the Buesching mastodon shows a series of arcuate concentrations of cementum defects, each centered on the ventral aspect of the tusk. The positions of these defects correspond with the spring season, starting as early as tusk year 24 (in which

there is a short arc, indicative of a minor battle), and continuing in each subsequent year at least through tusk year 31. We cannot determine from external inspection whether cementum defects developed in the spring of tusk year 23 or earlier, because this location has been altered by cementum remodeling associated with the formation of "periodontal pockets" (discussed below). This possibility could be tested by strategically positioned thin-sectioning, but we have not yet done this. Likewise, we cannot demonstrate that cementum defects formed in the same relative position in tusk year 32, because the proximal tusk margin that would contain them was not recovered.

The overall pattern of cementum defects, including the variable lengths of arcs of defects (with longer arcs presumably produced by greater impact forces at the tusk tip), is essentially identical to the pattern observed on the Hyde Park mastodon. We therefore interpret these features as indicative of recurring damage to the proximal margin of the tusk, sustained during musth battles that occurred during the early portion of spring. The timing of these battles is marked by "M"s (without asterisks) in Fig. S1b. In the Hyde Park mastodon and again in this specimen, this damage was severe enough to cause impairment of a cohort of newly differentiated odontoblasts and cementoblasts, resulting in subsequent formation of atypical dentin and cementum, respectively (3), but not severe enough to dislodge substantial fragments from the proximal margin of the tusk.

In addition to concentrated arcs of cementum defects, the Buesching mastodon's right tusk shows diffuse sets of cementum defects that seem to recur consistently in the late summer or autumn during adult years. (Fig. S1b). Tusk year 25 shows a small number of defects in summer and in either autumn or winter. Tusk year 26 shows a scattered array in autumn. Tusk year 27 shows an arcuate concentration much like the spring array, but in summer (possibly a late manifestation of musth behavior). Tusk year 28 shows a somewhat scattered array in the autumn, as do tusk years 29 and 30. As implied by the phrase "scattered array", this category of cementum defects shows gaps in distribution both longitudinally and circumferentially, suggesting that the episodes of tusk displacement that caused them were scattered in time and variable in both magnitude and direction of force. This in turn suggests that these defects formed when the tusk tip was used with a degree of fine-motor control, rather than an all-out assault.

f. Major battles

In addition to pointing out cementum defects and the relatively modest tusk damage they imply, we have already noted the much more dramatic fracture that removed the entire proximal margin of the right tusk of the Buesching mastodon (M** in Fig. S1b). We shall return to this shortly, specifically to consider its timing in more detail. However, we turn now to a fracture that may legitimately be called the "elephant in the room". This is indicated by a solid line, marked by "M*" in Fig. S1b and by white arrows in Fig. S2d. At first glance, this fracture might be easily dismissed as a postmortem phenomenon, possibly even sustained during removal of the tusk from its alveolus, or during transport or emplacement of the tusk in the pond environment where it was preserved.

However, this idea is definitively rejected by the simple experiment of running one's finger along the inside of the pulp cavity, immediately adjacent to the location of the fracture. Such action reveals an abnormally curved, but continuous deposit of dentin laminae, readily confirmed by visual inspection, that can only have formed post-fracture, in the summer and following months of tusk year 31. Because dentin does not remodel, it cannot "heal" in the sense that bone does, but it can be "welded" by deposition of new dentin laminae formed by a layer of odontoblasts that has "regrouped" following an injury and taken up dentin apposition anew. In this way, this fracture has been "welded" not only along its arc paralleling the proximal margin, but also along its long distal extension.

This damage is clearly much larger in scale than the tusk tip deflections that caused impingement of the ventral, growing margin of the tusk into the bony wall at the back of the alveolus, producing the arcs of cementum defects discussed above. However, we cannot explain the geometry of this much larger fracture with even a greatly intensified version of the same tusk movements responsible for cementum defects. Instead, to produce this type of fracture, it seems that the proximal extremity of the tusk – possibly only the dorsal arc of the growing margin – must have experienced a reaction force that drove it upward and forward (possibly also with a twisting component that would explain the distal diversion of the fracture). This combination of forces could have been produced by an enormous, posteriorly directed impact on the upwardly directed tusk tip, setting up a rotational moment that generated tension in the tusk base, opening up the fracture. The only scenario that seems capable of explaining this damage is one involving an opponent slamming one of his tusks into the Buesching mastodon's right tusk, rotating its tip backward relative to the rest of the mastodon's substantial mass.

The movements implied by the major break described above may also illuminate the genesis of a series of features near the gingival margin that we call "periodontal pockets" (Fig. S1b). Normally, the anteroventral portion of the tusk alveolus is a thin sheet of bone that, like all other parts of the alveolar wall, serves as the surface of origin for fibers of the periodontal ligament. This ligament is an extensive system of fibers that suspends the tusk dynamically within the alveolus. The thin sheet of bone near the ventral alveolar margin accommodates deformation, as when the tusk tip is deflected downward, but it generally recovers without serious injury, leaving the critical fibers of the periodontal ligament intact.

Periodontal pockets form when the tusk is displaced upward, tearing it away from periodontal ligament fibers (or their origin) near the ventral alveolar margin, allowing saliva, food particles, and other debris to enter a space that is normally a sealed, physiologically active, soft-tissue environment. Post-injury, the fluids, and perhaps the microbiology, of this wound setting appear to initiate inflammation of the affected soft tissue and resorption of the cementum surface, producing the shallow excavations that we identify as "pockets". Differential staining of regions within this system, combined with cross-cutting relationships of pocket boundaries, are the basis for distinguishing three successive stages of

healing of the pocket system. The pocket labelled with the dark gray tone (Fig. S1b), located at the proximal extremity of the system, apparently healed first, with new periodontal ligament fibers proliferating to close off the open space. The pocket with the medium gray tone appears to have closed next, and the pocket with the light gray tone may well have remained open at the time of the animal's death. Further interpretation must remain tentative. However, we suspect the dark gray pocket formed in conjunction with a tusk displacement like the one that produced the large fracture marked by white arrows in Fig. S2d, though occurring at an earlier time and possibly at a force level that was sub-critical for producing a fracture at the proximal end of the tusk. We similarly suspect that medium and light gray pockets formed simultaneously (after the dark gray pocket) and in conjunction with the major fracture discussed above. The medium gray represents a first stage of healing of this trauma, and the light gray maps an area of disrupted periodontal ligament that resulted from the major fracture and left periodontal support of the tusk still compromised at the time of the proximal perimeter fracture that occurred near the end of life. Finally, we suspect that the asymmetry of the medium and light gray pockets (a larger, but otherwise similar disruption of periodontal ligament compared to the dark gray pocket) is causally related to the geometry of the major fracture, which must have involved a torsional component of displacement relative to the normal position of this tusk.

The major fracture marked by white arrows in Fig. S2d must have formed after the time when dentin distal to the fracture had been added to the tusk. This is later than the spring timing of arcuate concentrations of cementum defects, which we associate with musth, but not necessarily much later. For instance, the major fracture could have formed in early summer, at a time when musth might still have been ongoing. Studies of second- and third-order dentinal lamination in the Hyde Park mastodon (3) show that a reduced rate of dentin apposition, consistent with the fasting behavior associated with musth in extant elephants (18), often lasts for two, or as many as three months. Musth and its behavioral correlates are thus not brief disturbances.

If asked to determine the timing of the proximal perimeter fracture (M** in Fig. S1b) that removed the entire growing margin, we would not have much to go on. The fracture itself propagated around the tusk circumference and was located just distal to any first-order periradicular feature marking the W/S boundary between tusk years 31 and 32. It therefore removed any cementum defects that may have formed shortly after this W/S boundary and any additional dentin deposited between the time of their formation and the time of death. Our $\delta^{18}O_p$ isotope data and thin section analyses are consistent with a death in early summer, which means the fracture could have been sustained during a musth battle late in the musth period of tusk year 32. A final and possibly key observation retrieves a detail from our earliest discussion of this tusk – the fact that as found, it had already sustained a complex fracture near the alveolar margin, breaking it into three pieces. The animal cannot have moved far under its own power without sacrificing the already-compromised integrity of this tusk, and we have no better explanation for this damage than the clashing tusks of two musth opponents.

Our ability to describe these events and their timing is still modest. Nevertheless, with (a) the periodontal injury indicated by the dark gray periodontal pocket, (b) the periodontal injury indicated by the medium gray and light gray pockets, together with the major fracture that disrupted dentin of year 31 (M* in Fig. S1b), and (c) the major fractures of the proximal perimeter (M** in Fig. S1b) and the body of the tusk near its alveolar margin, both of which appear to be associated with the end of life, we have a sequence of three events characterized by dynamically similar injuries. Earlier work has suggested stereotyped elements of fighting style in American mastodons (2, 3), and this new pattern of tusk fracture may represent another instance of this phenomenon.

Finally, given the consistent occurrence of autumn cementum defects in tusk years 25 through 30, why do they not occur in tusk year 31? If the summer of that year was the time when a major torsional fracture (white arrows in Fig. S2d) was sustained, this individual may have been making every effort to avoid use of his right tusk. The periodontal ligament for this tusk had been traumatized and while healing, may still have been sensitive to stress. If only to a modest degree, the absence of cementum defects in tusk year 31 supports our provisional interpretation of musth-battle-induced damage to this tusk.

g. Cause of death

In addition to the proximal perimeter fracture of the right tusk, a major circular perforation of the right temporal fossa of the Buesching mastodon closely matches damage discovered on other adult males that died at the same time of year and have been interpreted as victims of musth battles (2, 3). Severe tusk and cranial damage to the Buesching mastodon, which both occurred to the right side of the face, were likely generated during the same or closely spaced events, and are consistent with damage inflicted by blows from another male mastodon. Parallel investigation of the Hyde Park mastodon (3) leaves little doubt that the Buesching mastodon succumbed to injuries sustained in a musth battle. This type of damage can be explained as a deeply penetrating wound produced by vigorous thrusting of a tusk tip into the head of an opponent. The damage location makes interruption of the carotid supply of blood to the brain a likely outcome.

h. Biogenicity of isotope data

Compared to enamel, dentin is more susceptible to diagenetic alteration of original isotope values, particularly in deeper-time fossils (20, 21). However, a long history of isotope analyses of late Pleistocene proboscidean tusk dentin has shown biogenicity of isotopes ($\delta^{18}O$, $\delta^{13}C$, $\delta^{15}N$) preserved in dentin carbonate from a variety of depositional settings, including ones similar to the Buesching deposit (6, 22–24). However, as a precaution, we evaluated $\delta^{18}O$ using the phosphate component of dentin, which is particularly robust to diagenesis (23). All $^{87}Sr/^{86}Sr$ measurements presented here come from the hydroxylapatite of the same well-preserved serial samples of tusk dentin that yielded $\delta^{18}O$ values.

As we explore in the results of the main text, while there are concerns that dentin $^{87}Sr/^{86}Sr$ may be susceptible to diagenetic alteration (25, 26), the cyclic

variability in our results (for both $\delta^{18}O$ and $^{87}Sr/^{86}Sr$) and alignment between isotope values and physical features of the tusk both indicate that our measured values are biogenic. Tusk $\delta^{18}O$ values were highly cyclic, with dark-light (winter-spring) boundaries of dentin consistently corresponding to local minima in $\delta^{18}O$. This differs strongly from the expectation of diagenetically altered isotope values, which should be largely homogeneous or random across a time series (27). Thus, our reported $\delta^{18}O$ values probably represent original (biologic) values. We also find dramatic changes in $^{87}Sr/^{86}Sr$ along the time series, including annual cyclicity as an adult (Fig. 1). This cyclicity argues that tusk $^{87}Sr/^{86}Sr$ are also biogenic. Further, although we find relatively stable $^{87}Sr/^{86}Sr$ (mean = 0.70933, standard deviation = 2.7×10^{-5}) in the early portion of adolescence (Stage *i*), these values are distinct from where the fossil was recovered ($^{87}Sr/^{86}Sr$ = 0.70983) and are unlikely to have originated through diagenetic replacement.

i. Probabilities of movement, model strengths, and future advances

As described in the main manuscript (Materials and Methods), movement between serial samples is modeled using distances between PRO centroids of successive serial samples and the proportion of high-probability locations (pixels) in each PRO (analogous to relative area of the PROs). State-space modelling is a natural fit for evaluating $^{87}Sr/^{86}Sr$ time series because it can directly model the movement of an individual when multiple pathways are possible (28, 29). Just as animals move across landscapes, our model proceeds linearly through time as it estimates the most likely changes in landscape use, given multiple possible solutions. While the temporally linear nature of the model is similar to actual animal movements through time, a possible model improvement might be to estimate movements using greater numbers of time slices (e.g., simultaneously incorporating T+1, T+2, … T+n). While deviating from the purely linear nature of movement, Bayesian inference that utilizes "future" values of tusk $^{87}Sr/^{86}Sr$ as priors may improve the accuracy with which we can reconstruct landscape use by extinct organisms. Another possible improvement to our model would be to formally incorporate the mixing of geographically proximate isoscape $^{87}Sr/^{86}Sr$ values when calculating the probability of occupancy. Incorporating spatial averaging of bioavailable $^{87}Sr/^{86}Sr$ by mastodons, however, relies on estimating the size of daily to monthly geographic ranges during foraging and other behaviors, and understanding how those ranges may change due to the age of an individual, its sex, and seasons of dentin formation. Results presented here from our more conservative model (i.e., with fewer parameters) provide useful initial estimates for parameterizing future models.

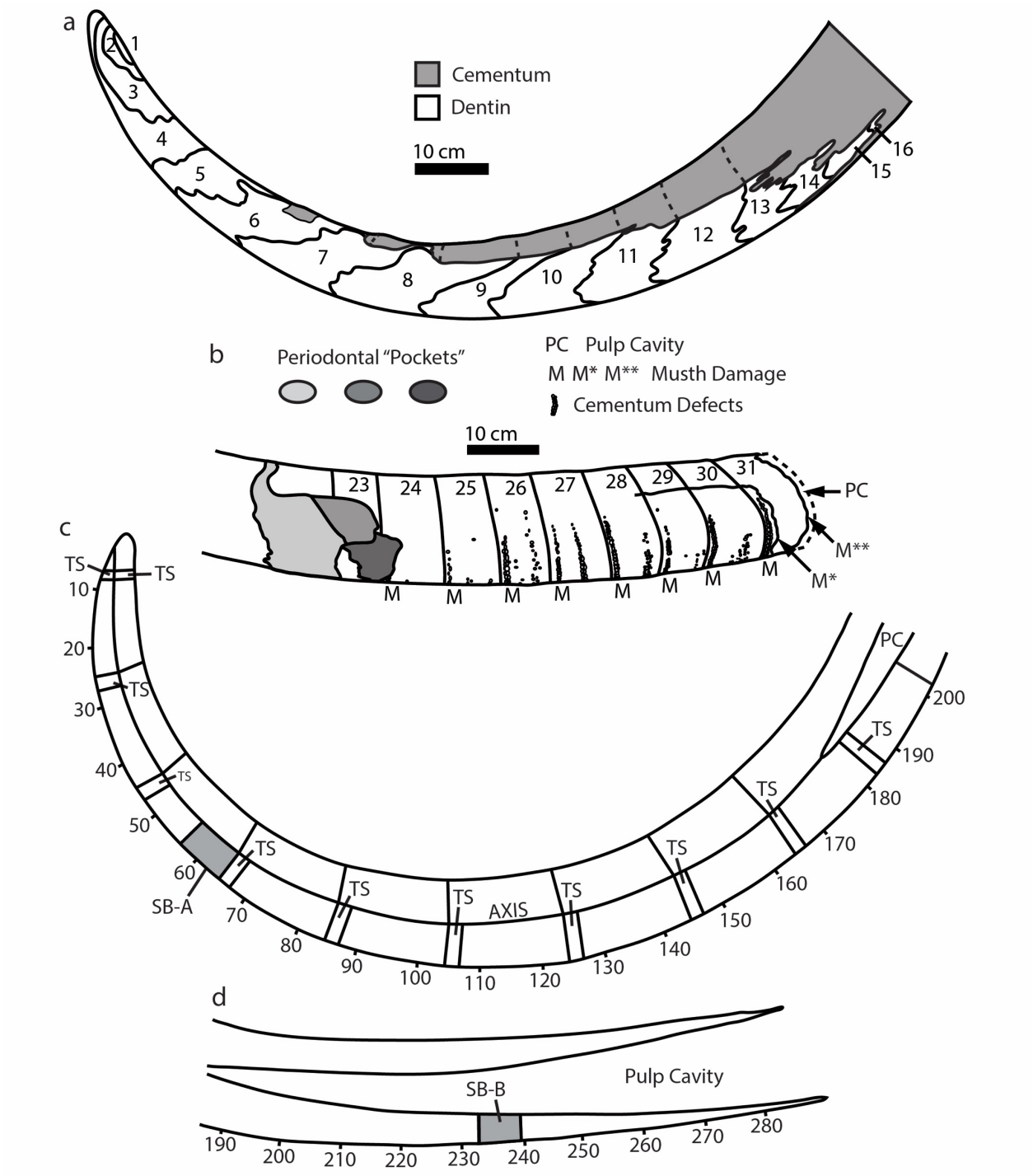

Figure S1. Right tusk of the Buesching mastodon. (**a**) Distal portion, showing ventromedial surface. Numbers identify tusk years 1-16, the only years with dentin exposure on this part of the tusk. Years demarcated by solid lines tracing exposed winter-spring boundaries, and by dashed lines where boundaries extend

under intact cementum. (**b**) Ventromedial surface of proximal portion of tusk. Numbers identify years demarcated by solid lines following periradicular features (see Supplementary Discussion 2e) associated with winter-spring boundaries. Periodontal “pockets” (Supplementary Discussion 2f) shown in three shades of gray. Minor musth damage (Ms without asterisks along lower margin) consists of arcuate concentrations of cementum defects occurring soon after winter-spring boundaries; more diffuse sets of cementum defects occur later in most years. Solid line in tusk year 31 and extending distally into tusk year 28 is a large fracture, marked with an arrow and M*, that formed during early summer of tusk year 31. Arrow labelled PC indicates opening of pulp cavity; nearby finely dashed line indicates reconstructed proximal margin; existing proximal margin was formed during early portion of tusk year 32 by another major fracture and is marked by an arrow and M**. (**c**) Medial view of axial slab extracted from distal 2 m of tusk. Solid, curved lines indicate slab margins (distance from tusk tip, in cm, marked along ventral edge), pulp cavity (PC) margins, and tusk axis. Solid, straight lines indicate cuts made to separate axial slab into segments and blocks used for thin sections (TS) and serial sampling for isotope analysis. Sample block SB-A (gray) was used to sample adolescent years in this study. (**d**) Medial view of axial slab (dorsal and ventral moieties) extracted from proximal meter of tusk. Labels as for (c); sample block SB-B (gray) was used to sample adult years in this study.

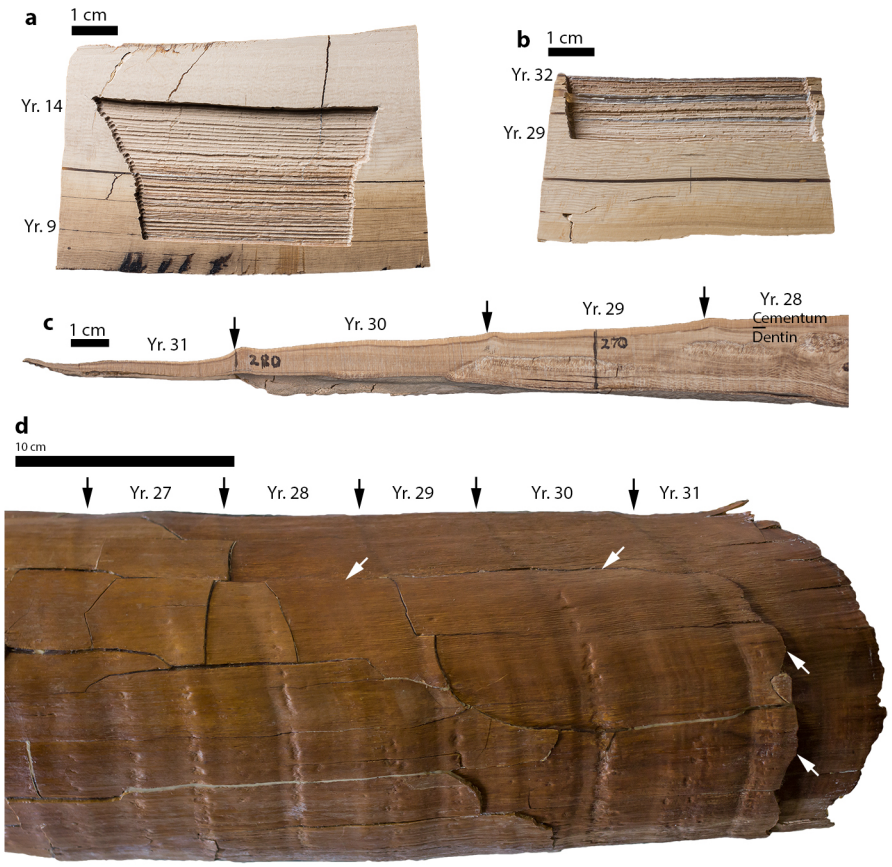

Figure S2. Key portions of the Buesching mastodon's right tusk. Photographs show parts of the axial slab and ventromedial surface of the proximal tusk. (**a**) Sample block used for serial sampling of adolescent years (medial surface of SB-A in Fig. S1c; proximal toward right). Mill paths shown, with lighting from upper left (sample order: high→low, tusk year 14→9). (**b**) Sample block used for serial sampling of adult years near end of life (medial surface of SB-B in Fig. S1d; proximal toward right). Pulp cavity surface along upper margin, lighting from upper left (sample order: high→low, tusk year 32→29). (**c**) lateral surface of dorsal moiety of axial slab from proximal portion of tusk; external cementum surface along upper margin; pulp cavity surface along lower margin. Arrows along upper margin indicate locations of winter-spring boundaries associated with periradicular bands. Year labels mark progress of tusk extension (length increase) along outer surface. (**d**) Ventromedial view of external surface of proximal end of tusk. Locations of winter-spring boundaries and periradicular bands indicated by arrows along upper margin. Major break sustained in early summer of tusk year 31 indicated with white arrows (and solid line in Fig. S1b). Margin at right edge of image was produced by another major fracture that separated the actual proximal margin from the rest of the tusk.

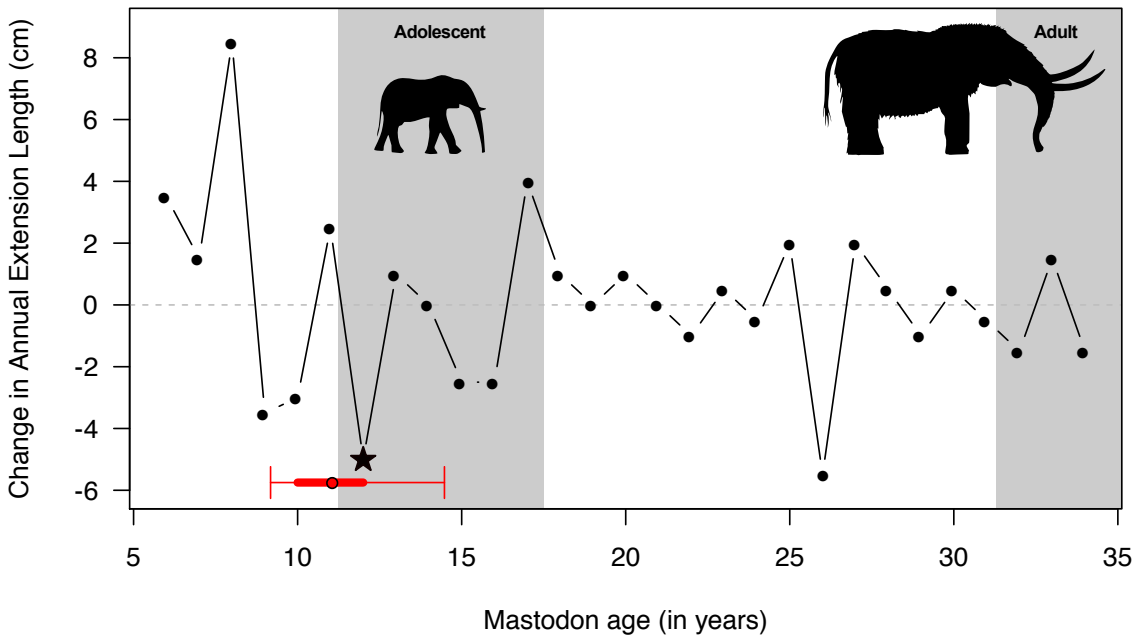

Figure S3. Differences between successive values of annual extension length measured on the Buesching mastodon's right tusk. Measurements (in cm) taken between winter/spring boundaries. Mastodon age estimated by adding 3 to each tusk year (see text for details). Expectation for age-of-eviction based on previous evaluations of male mastodons (2) shown as mean (red point), interquartile range (thick horizontal red line), and 95% confidence interval (horizontal error bars). Horizontal dashed line (at 0.0) separates years with year-to-year increases (above the line) and decreases (below the line) in extension length. There is a sharp reduction in extension length between mastodon ages 11 and 12 (tusk years 8 and 9) likely due to unusual nutritional stress. Thus, age 12 (tusk year 9; star) is interpreted as the year of eviction from the natal herd. Following age 12, annual changes in extension length are both positive and negative, but largely stabilize following high growth during age 17 (tusk year 14). Annual extension length for age 35 (tusk year 32) cannot be calculated because it is incomplete due to a tusk fracture that is probably associated with the mastodon's death. Shaded regions indicate ages sampled for this study.

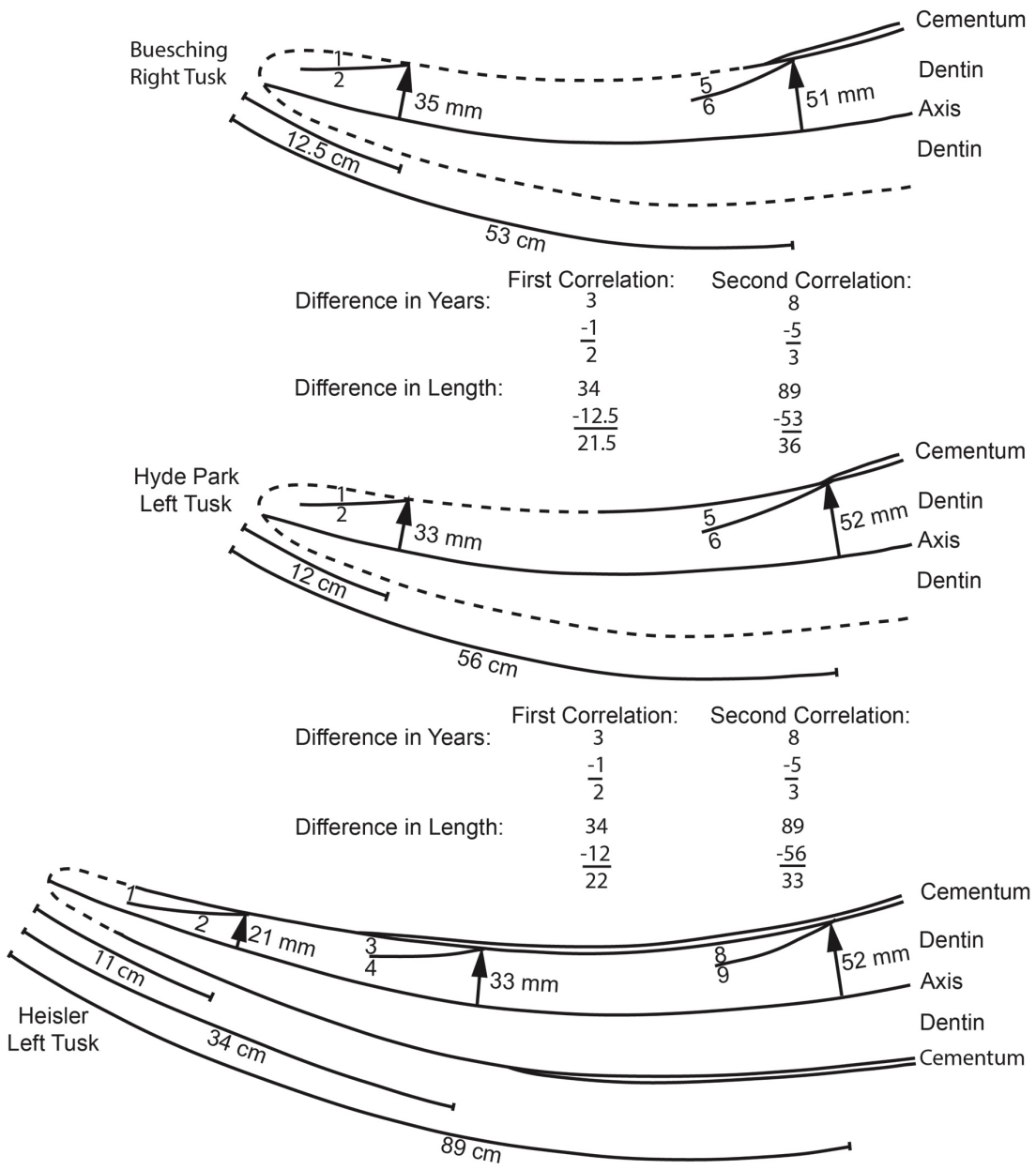

Figure S4. Estimating numbers of years lost from tusk tips. Schematic diagrams of tusk tips of Buesching (this paper), Hyde Park (3), and Heisler (3) mastodons. Comparisons illustrate how we estimate the number of early years lost by tip breakage in tusks of older mastodons. Outlines represent tusk structure in longitudinal, axial section. Tusk axis shown as a solid line located roughly midway between dorsal and ventral margins. Solid lines along tusk margins represent outer and inner surfaces of cementum, or dentin surfaces that approximate the dentin-cementum junction. Dashed lines along tusk margins indicate regions where tip abrasion has clearly truncated dentin. Measurements and comparisons used for correlation discussed in Supplementary Discussion 2c.

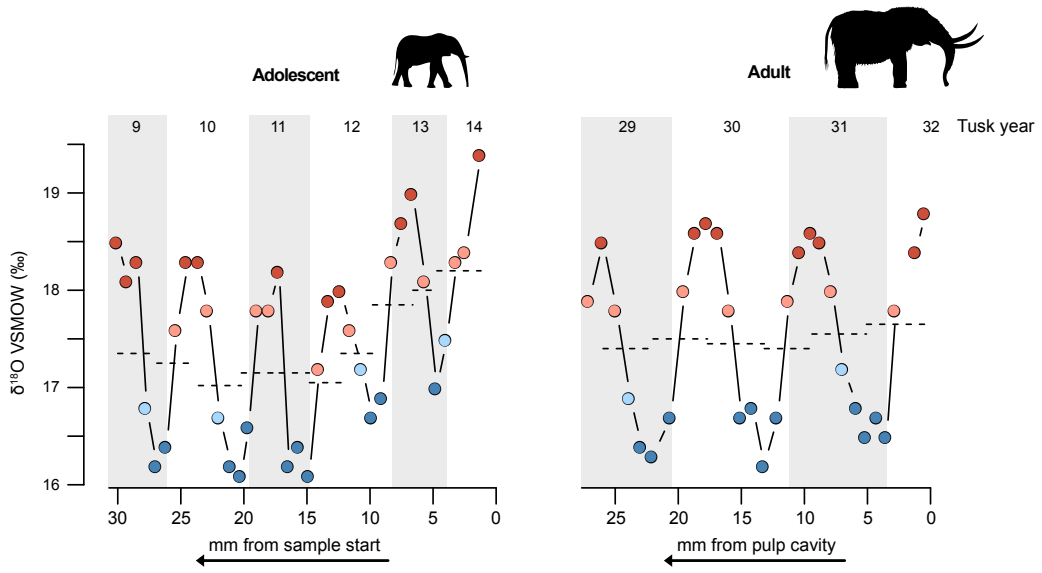

Figure S5. Determining growth season for serial tusk samples. Semi-annual means between semi-annual high and low $\delta^{18}O_p$ (dashed lines on rising and falling limbs of the plot) are used to separate warm-season (higher-than-average $\delta^{18}O_p$, red) and cool-season (lower-than-average $\delta^{18}O_p$, blue) serial samples. Darker shades of red and blue based on $\delta^{18}O_p$ z-score; $\delta^{18}O_p$ z-score ≥ 0.75 (summer) and $\delta^{18}O_p$ z-score ≤ -0.75 (winter). Tusk years indicated across top edge of plot, with boundaries indicated by edges of alternating gray and white panels. Horizontal axis shows ending positions of serial samples (in mm) from the start of each sequence. Arrows below plots indicate order of sample acquisition.

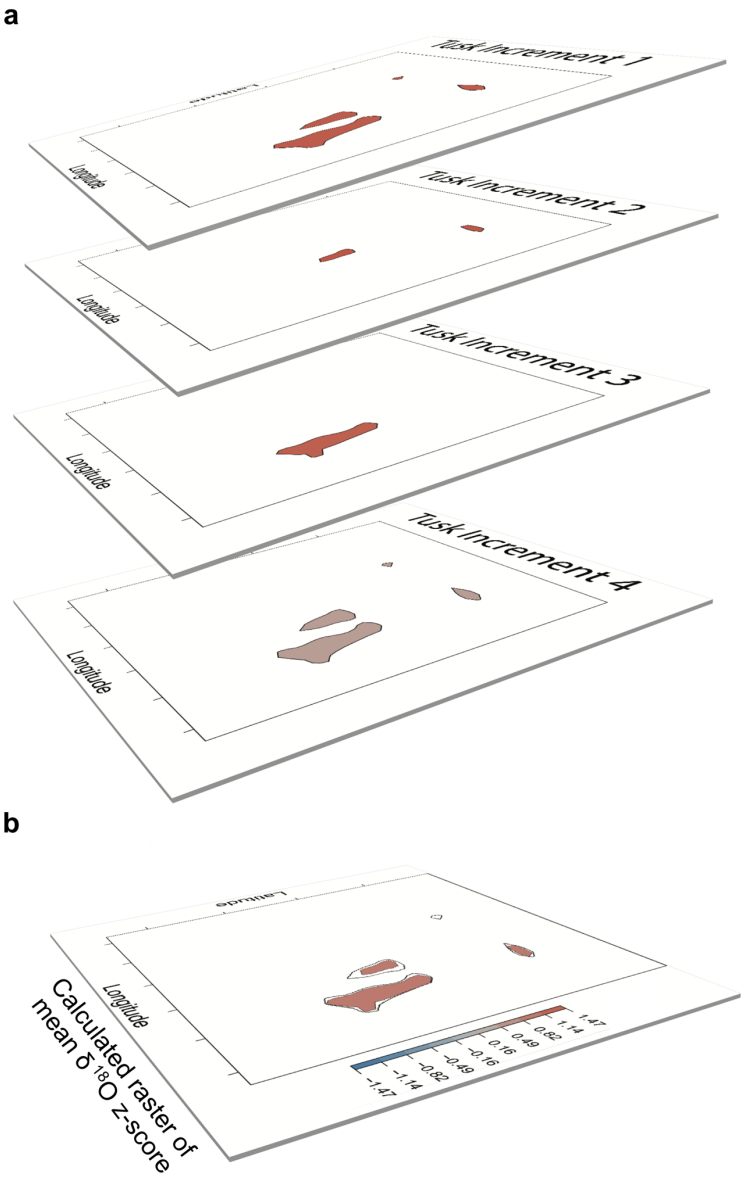

Figure S6. Schematic diagram showing superimposition and calculation of mean $\delta^{18}O_p$ z-scores across Potential Regions of Occupancy. (**a**) Potential Regions of Occupancy (PRO) for each serial sample are defined using a kernel density estimator. Each pixel within the PRO is assigned the $\delta^{18}O_p$ z-score for that serial sample. (**b**) Calculated mean $\delta^{18}O_p$ z-scores across space (calculated separately for the adolescent and adult datasets). Means are not calculated for locations (pixels) overlapped by fewer than three PROs (unshaded regions in b) due to low sample size and because they do not indicate areas of recurring use. Color-scale is the same for $\delta^{18}O_p$ z-score (a) and mean $\delta^{18}O_p$ z-score (b).

a

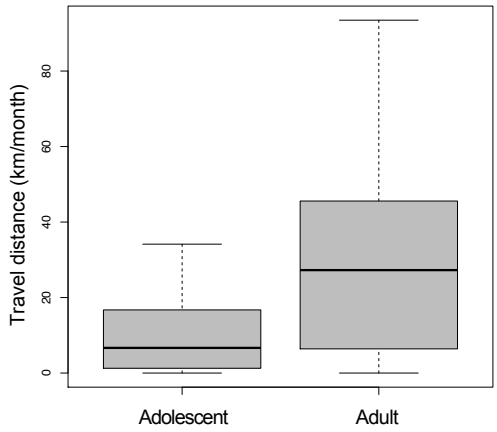

b

Kernel Density Threshold	Median distance traveled (km/month)		Mann-Whitney U test
	Adolescent	Adult	
75%	6.7	27.3	U = 248, p < 0.01**
90%	7.8	16.1	U = 316, p = 0.016*

Figure S7. Distribution of distances moved between consecutive serial samples during adolescence and adulthood. Distances standardized to time (in months) between samples, based on serial sample thickness (relative to total tusk year thickness). (**a**) Distances estimated using great circle distances between PRO centroids with the highest supported occupancy between serial samples. Travel distances are significantly larger during adulthood ($p < 0.01$). (**b**) Sensitivity analyses of results (in (a)) using the most highly spatially concentrated 90% of high-probability isoscape values for generating PROs. Spatial concentrations evaluated using a kernel density estimator (KDE). The model is parameterized using the 75% KDE and further tested using the 90% KDE threshold. Test significance indicated as $p < 0.01$ (**) and $p < 0.05$ (*).

a

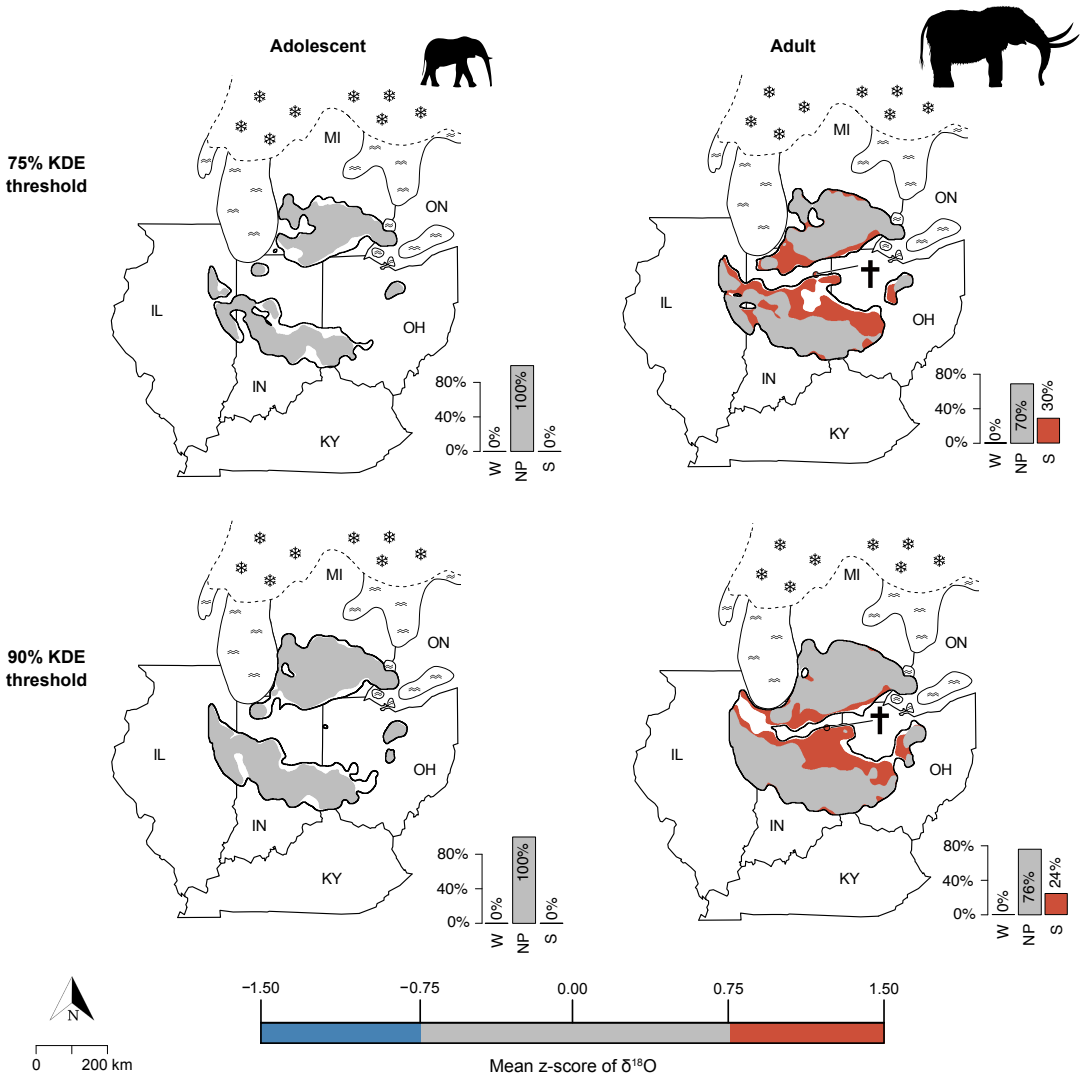

b

Kernel Density Threshold	Adolescent			Adult		
	Winter	No preference	Summer	Winter	No preference	Summer
75%	1 (0%)	56,925 (100%)	4 (0%)	9 (0%)	69,932 (70%)	30,271 (30%)
90%	4 (0%)	80,205 (100%)	0 (0%)	22 (0%)	93,388 (76%)	30,079 (24%)

Figure S8. Sensitivity analysis of seasonal preferences in geographic use based on mean $\delta^{18}O_p$ z-scores of superimposed Potential Regions of Occupancy (PRO; as illustrated in Fig. S7). (**a**) Results calculated using the most highly concentrated 75%, and 90% of high-probability isoscape values (top and bottom rows, respectively), for adolescence (left column) and adulthood (right column). Results in top row (a) illustrated previously (Fig. 2). Inset histograms show proportion of pixels identified as summer-use (S), winter-use (W), or no

preference (NP). Red = summer ($\delta^{18}O_p$ z-scores $\geq$ 0.75), blue = winter ($\delta^{18}O_p$ z-scores $\leq$ -0.75), gray = no preference. Dashed boundary (and snowflakes) identify glacial margin (30). Wavy lines identify lakes (30). (**b**) Table summarizing inset histograms of (a), including pixel counts (and percentages) of summer-use, winter-use, or no seasonal preference. Consistent across the sensitivity analysis, strong seasonal preferences are only recovered during adulthood and only for warm season landscape use (red-shaded polygons).

a

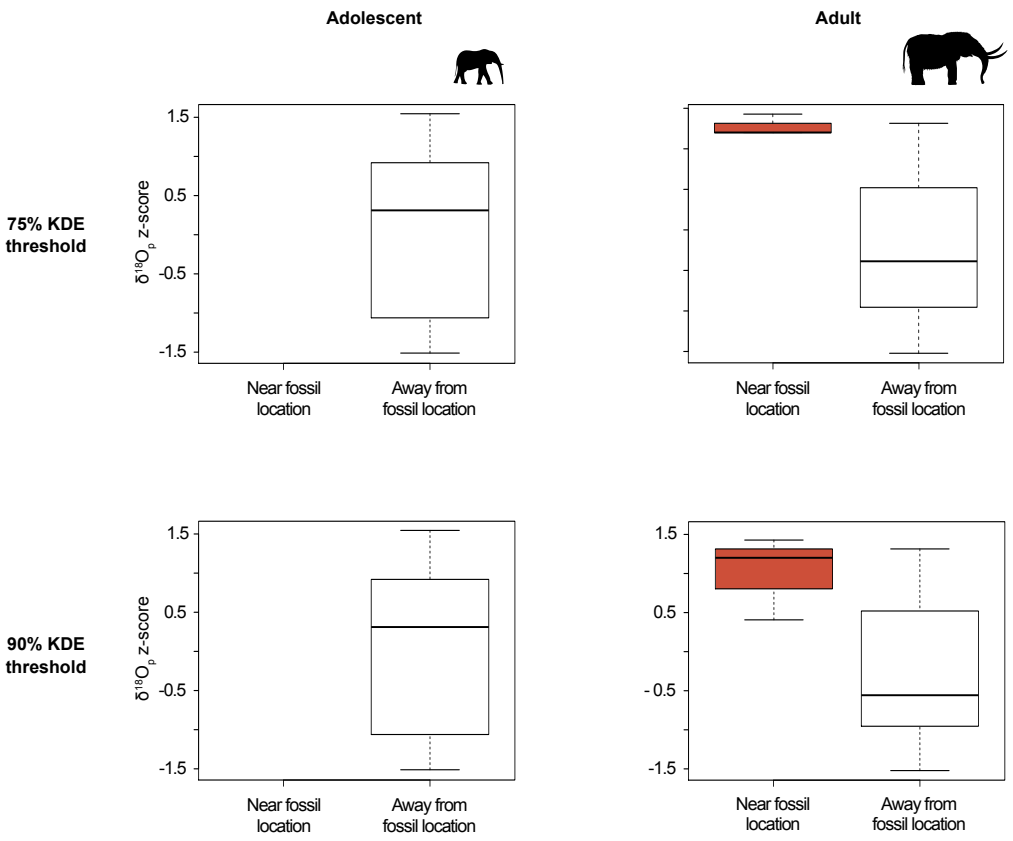

b

Kernel Density Threshold	Comparison of $\delta^{18}O_p$ z-score (when Near vs. Away from the fossil location)	
	Adolescent	Adult
75%	---	U = 72, p = 0.011 *
90%	---	U = 85.5, p = 0.015 *

Figure S9. Sensitivity analyses for seasonality in landscape use during adolescence and adulthood. (**a**) Comparisons evaluate the distribution of $\delta^{18}O_p$ z-scores attributable to mastodon occupation of regions "near" versus "far" from the recovery location of the Buesching mastodon during adolescence and adulthood. Here, "near" is defined as being within one-month's travel distance (see Fig. S7b for distances). Results are the same if the larger adult travel distances are used to evaluate the adolescent datasets. Regional occupancy based on the most highly supported Potential Region of Occupancy (PRO) for each serial sample (as in Fig. 4). Results provided using two spatial concentration thresholds of $^{87}Sr/^{86}Sr$ tusk-isoscape matches for generating PROs: most highly spatially concentrated 75% (top row), and 90% (bottom row). Spatial concentrations evaluated using a kernel density estimator (KDE). For each buffer, the model is parameterized using the 75% KDE and further tested using the 90% KDE

threshold. (**b**) Table of Mann-Whitney U tests for comparisons shown in (a). Level of statistical significance indicated as $p < 0.05$ (*).

Dataset S1

Annual extension lengths for years of growth preserved in the Buesching mastodon's right tusk. Lengths measured between winter/spring boundaries along the tusk. See Supplementary Methods and Supplementary Discussion for details.

Dataset S2

Serial sampling metadata and isotope data. "BU3" samples are from adolescence (sampled from SB-A, Fig. S1). "BU2" samples are from adulthood (sampled from SB-B, Fig. S1). "Sample thickness (mm)" reflects dimensions of mill paths of serial samples. See Supplementary Methods and Supplementary Discussion for details.

SI References

1. C. Widga, *et al.*, Late Pleistocene proboscidean population dynamics in the North American Midcontinent. *Boreas* **46**, 772–782 (2017).

2. D. C. Fisher, "Paleobiology and extinction of proboscideans in the Great Lakes Region of North America" in *American Megafaunal Extinctions at the End of the Pleistocene*, 3rd Ed., G. Haynes, Ed. (Springer, Dordrecht, 2009), pp. 55–75.

3. D. C. Fisher, "Taphonomy and paleobiology of the Hyde Park mastodon" in *Mastodon Paleobiology, Taphonomy, and Paleoenvironment in the Late Pleistocene of New York State: Studies on the Hyde Park, Chemung, and North Java Sites*, W. D. Allmon, P. L. Nester, Eds. (Palaeontographica Americana, 2008), pp. 197–289.

4. K. M. Smith, D. C. Fisher, Sexual dimorphism of structures showing indeterminate growth: tusks of American mastodons (*Mammut americanum*). *Paleobiology* **37**, 175–194 (2011).

5. R. M. Laws, Age criteria for the African elephant, *Loxodonta a. africana*. *E. Afr. Wildl. J.* **4**, 1–37 (1966).

6. D. C. Fisher, "Season of death of the Hiscock mastodonts" in *Late Pleistocene and Early Holocene Paleoecology and Archeology of the Eastern Great Lakes Region*, R. S. Laub, N. G. Miller, D. W. Steadman, Eds. (Bull. Buffalo Soci. Nat. Sci., 1988), pp. 115–125.

7. D. C. Fisher, Paleobiology of Pleistocene proboscideans. *Annu. Rev. Earth Planet. Sci.* **46**, 229–260 (2018).

8. D. C. Fisher, “Mastodont procurement by Paleoindians of the Great Lakes region: hunting or scavenging?” in *The Evolution of Human Hunting*, M. H. Nitecki, D. V. Nitecki, Eds. (Plenum Publishing Corp., 1987), pp. 309–421.

9. D. C. Fisher, “Extinction of proboscideans in North America” in *The Proboscidea: Evolution and Palaeoecology of Elephants and Their Relatives*, J. Shoshani, P. Tassy, Eds. (Oxford University Press, 1996), pp. 296–315.

10. C. J. Moss, *Elephant Memories: Thirteen Years in the Life of an Elephant Family* (William Morrow, 1988).

11. D. C. Fisher, S. G. Beld, A. N. Rountrey, “Tusk record of the North Java mastodon” in *Mastodon Paleobiology, Taphonomy, and Paleoenvironment in the Late Pleistocene of New York State: Studies on the Hyde Park, Chemung, and North Java Sites*, W. D. Allmon, P. L. Nester, Eds. (Palaeontographica Americana, 2008), pp. 417–463.

12. P. L. Koch, D. C. Fisher, D. Dettman, Oxygen isotope variation in the tusks of extinct proboscideans: a measure of season of death and seasonality. *Geology* **17**, 515–519 (1989).

13. B. E. Crowley, J. H. Miller, C. P. Bataille, Strontium isotopes ($^{87}Sr/^{86}Sr$) in terrestrial ecological and palaeoecological research: empirical efforts and recent advances in continental-scale models. *Biol. Rev.* **92**, 43–59 (2017).

14. C. P. Bataille, *et al.*, A bioavailable strontium isoscape for Western Europe: a machine learning approach. *PLoS ONE* **13**, e0197386 (2018).

15. C. P. Bataille, B. E. Crowley, M. J. Wooller, G. J. Bowen, Advances in global bioavailable strontium isoscapes. *Palaeogeogr. Palaeocl.* **555**, 109849 (2020).

16. J. J. El Adli, M. D. Cherney, D. C. Fisher, J. M. Harris, Last years of life and season of death of a Columbian mammoth from Rancho La Brea. *Nat. Hist. Mus. Los Angeles County Sci. Series* **42**, 65–80 (2015).

17. G. Haynes, *Mammoths, Mastodonts, and Elephants: Biology, Behavior, and the Fossil Record* (Cambridge University Press, 1991).

18. J. H. Poole, Cynthia J. Moss, Musth in the African elephant, *Loxodonta africana*. *Nature* **292**, 830–831 (1981).

19. L. A. Taylor, *et al.*, Movement reveals reproductive tactics in male elephants. *J. Anim. Ecol.* **89**, 57–67 (2020).

20. Y. Wang, T. E. Cerling, A model of fossil tooth and bone diagenesis: implications for paleodiet reconstruction from stable isotopes. *Palaeogeogr. Palaeocl.* **107**, 281–289 (1994).

21. T. Tütken, T. W. Vennemann, Fossil bones and teeth: Preservation or alteration of biogenic compositions? *Palaeogeogr. Palaeocl.* **310**, 1–8 (2011).

22. D. C. Fisher, D. L. Fox, "Season of death and terminal growth histories of the Hiscock mastodons" in *Hiscock Site: Late Pleistocene and Holocene Paleoecology and Archaeology of Western New York State*, Bull. Buffalo Soci. Nat. Sci., R. S. Laub, Ed. (2003), pp. 83–101.

23. D. C. Fisher, D. L. Fox, "Season of death of the Dent mammoths: distinguishing single from multiple mortality events" in *Frontiers in Colorado Paleoindian Archaeology: From the Dent Site to the Rocky Mountains*, R. H. Brunswig, B. L. Pitblado, Eds. (University Press of Colorado, 2007), pp. 343–377.

24. D. C. Fisher, D. L. Fox, "Five years in the life of an Aucilla River mastodon" in *First Floridians and Last Mastodons: The Page-Ladson Site in the Aucilla River*, S. D. Webb, Ed. (Springer Netherlands, 2006), pp. 343–377.

25. B. K. Nelson, M. J. DeNiro, M. J. Schoeninger, D. J. De Paolo, P. E. Hare, Effects of diagenesis on strontium, carbon, nitrogen and oxygen concentration and isotopic composition of bone. *Geochem. Cosmochim. Acta* **50**, 1941–1949 (1986).

26. P. Budd, J. Montgomery, B. Barreiro, R. G. Thomas, Differential diagenesis of strontium in archaeological human dental tissues. *Appl. Geochem.* **15**, 687–694 (2000).

27. K. A. Hoppe, P. L. Koch, T. T. Furutani, Assessing the preservation of biogenic strontium in fossil bones and tooth enamel. *Int. J. Osteoarchaeol.* **13**, 20–28 (2003).

28. N. A. Cressie, *Statistics for Spatial Data* (John Wiley & Sons, Inc., 1993).

29. T. Patterson, L. Thomas, C. Wilcox, O. Ovaskainen, J. Matthiopoulos, State–space models of individual animal movement. *Trends Ecol. Evol.* **23**, 87–94 (2008).

30. A. S. Dyke, An outline of North American deglaciation with emphasis on central and northern Canada. *Geochem. Cosmochim. Acta* **2**, 373–424 (2004).